Universal interrogation protocol with zero probe-field-induced frequency shift for quantum clocks and high-accuracy spectroscopy

T. Zanon-Willette* and R. Lefevre
LERMA, Observatoire de Paris, PSL Research University, CNRS, Sorbonne Universités, UPMC Université de Paris 06, F-75005 Paris, France

A. V. Taichenachev and V. I. Yudin
Novosibirsk State University, ul. Pirogova 2, Novosibirsk 630090, Russia and Institute of Laser Physics, SB RAS, pr. Akademika Lavrent'eva 13/3, Novosibirsk 630090, Russia

(Received 28 February 2017; revised manuscript received 7 June 2017; published 8 August 2017)

Optical clock interrogation protocols, based on laser-pulse spectroscopy, suffer from probe-induced frequency shifts and their variations induced by laser power. The original hyper-Ramsey probing scheme, which was proposed to alleviate those issues, does not fully eliminate the shift, especially when decoherence and relaxation by spontaneous emission or collisions are present. We propose to solve the fundamental problem of frequency shifts induced by the laser probe by deriving the exact canonical form of a multipulse generalized hyper-Ramsey resonance, including decoherence and relaxation. We present a universal interrogation protocol based on composite laser-pulse spectroscopy with phase modulation eliminating probe-induced frequency shifts at all orders in the presence of various dissipative processes. Unlike frequency shift extrapolation based methods, a universal interrogation protocol based on $\pm\pi/4$ and $\pm 3\pi/4$ phase-modulated resonances is proposed which does not compromise the stability of the optical clock while maintaining an ultrarobust error signal gradient in the presence of substantial uncompensated ac Stark shifts. Such a scheme can be implemented in two flavors: either by inverting clock state initialization or by pulse order reversal even without a perfect quantum state initialization. This universal interrogation protocol can be applied to atomic, molecular, and nuclear frequency metrology, mass spectrometry, and the field of precision spectroscopy. It might be designed using magic-wave-induced transitions, two-photon excitation, and magnetically induced spectroscopy or it might even be implemented with quantum logic gate circuit and qubit entanglement.

DOI: 10.1103/PhysRevA.96.023408

I. INTRODUCTION

Atomic optical clocks are recognized to be ideal platforms for highly accurate frequency measurements, leading to very stringent tests of fundamental physical theories [1], such as relativity [2,3], detection of gravitational waves [4], possible variation of fundamental constants with time [5], or the search for dark matter [6]. Depending on the selected atomic species used to achieve stable and accurate optical frequency standards, single trapped ion clocks [7,8] and neutral atom lattice clocks [9–11] have been characterized over many years, reducing systematic uncertainties to a fractional frequency change well below 10^{-16}, surpassing current microwave atomic frequency standards. These promising standards are based on ultranarrow electric-dipole-forbidden transitions. For ions, examples are spin-forbidden transitions using quantum logic spectroscopy [12], or electric-quadrupole or octupole transitions, as in the single $^{171}Yb^{+}$ ion clock which has recently demonstrated a relative 3×10^{-18} systematic uncertainty [13]. Optical lattice clocks with alkaline-earth-like atoms are based on a doubly forbidden transition weakly allowed in fermions (odd isotopes) by a level mixing due to the hyperfine structure. ^{171}Yb and ^{87}Sr optical lattice clocks are now reaching relative stabilities in the 10^{-16} range [14] and relative accuracies of 2×10^{-18} [15], potentially leading to a redefinition of the second for the next decade [16,17]. Strongly forbidden transitions, with vanishing spin-orbit coupling due to zero nuclear spin, have been studied more recently in bosonic species (^{88}Sr, ^{174}Yb, ^{24}Mg), but they require a two-photon excitation technique [18,19] or a magnetically induced spectroscopy [20–23], which are both limited by important ac Stark shifts or Zeeman frequency shifts. Because the quest for extreme precision in ultrahigh-resolution spectroscopy is still progressing, it will ultimately require new laser stabilization protocols, reducing systematic uncertainties to very low levels, pushing precision even further. Among these uncertainties, frequency shifts from the laser probe itself are always present and might become a severe limitation for the next generation of fermionic and bosonic quantum clocks with fractional frequency change below 10^{-18}.

Ramsey spectroscopy [24] was first modified by including a frequency step during the laser pulses in order to compensate the probe-induced frequency shift [25]. However, when the shift is not fully compensated, a frequency shift remains, with a linear dependence to the error on the compensation. Then, composite laser pulse techniques, so-called hyper-Ramsey (HR) spectroscopy, previously developed in nuclear magnetic resonance and quantum computation [26–28], were applied with electromagnetic phase-modulated resonances [29–31] in order to provide nonlinear elimination of residual uncompensated light-shift contributions and laser power variations [32–35]. Such an HR spectroscopy has been successfully applied on the ultranarrow electric octupole transition of the single $^{171}Yb^{+}$ ion, reducing ac Stark shifts by four orders of magnitude, and has proven to be shielded from small pulse area

*thomas.zanon@upmc.fr

variations [36]. To completely remove the third-order weak dependence of the HR clock frequency shift on light-shift uncompensated parts, a modified hyper-Ramsey technique (MHR) was experimentally implemented within a bosonic ^{88}Sr lattice clock, demonstrating the suppression of the 2×10^{-13} probe Stark shifts to below 10^{-16}, drastically expanding the acceptance bandwidth of imperfect shift compensation [37].

However, it has been pointed out that the reliability of interrogation schemes against uncompensated probe frequency shifts and laser power variations might be severely limited by decoherence, compromising the improvements of further metrological performances [38].

We manage to overcome this fundamental obstacle by building an ultrarobust clock-laser stabilization scheme taking into account atomic decoherence and relaxation by both spontaneous emission and weak collisions. The error signal is synthesized by repeating and combining several atomic population excitation fraction measurements, interleaved by a controllable population inversion between clock states. The paper is organized as follows: We begin by presenting the two-level optical Bloch equations which are used to describe coherent interaction between laser and atoms including several dissipative processes which may disrupt the clock transition. The Bloch vector resulting from a multipulse generalized hyper-Ramsey (GHR) resonance is first expressed in a canonical form with a clock frequency shift. Note that our formal analytic (GHR) resonance pattern can integrate additional NMR rotation composite pulse protocols [26] to remove any potential additional errors if desired. The corresponding error signal line shape is then derived and the associated clock frequency shift is obtained by a combination of phase-modulated (GHR) resonances. We introduce a general 2D diagram approach for frequency shift reconstruction allowing a global map analysis of decoherence and relaxation effects. The main part of this paper is dedicated to a universal laser interrogation protocol using a combination of multiple (GHR) error signals based on $\pi/4,3\pi/4$ phase steps and quantum state initialization generating a laser frequency locking point which is immune to probe-induced frequency shifts. We finally explore and compare the sensitivity of the original HR interrogation protocol, such as applied to the single ion ^{171}Yb$^+$ clock [36], to our universal laser frequency stabilization technique for different radiative configurations of a two-level clock transition.

II. CANONICAL FORM FOR ANALYTICAL MULTIPULSE (GHR) RESONANCE EXPRESSION

To design a universal interrogation protocol for fermions and bosons, we first derive the exact analytical expression of a phase-modulated generalized hyper-Ramsey (GHR) resonance along with the clock frequency shift expression, including dissipative processes [39,40]. The atomic transition, shown in Fig. 1 , includes a decoherence term γ_c, a spontaneous emission rate denoted Γ, and an excited state population relaxation ξ induced by weak collisions. Bloch variables are used to describe the fraction of population excitation after successive optical composite pulses with area θ_l indexed by $l = 1,\ldots,k,\ldots,n$, including a free evolution time T at index $l = k$. Light pulse duration $\tau_{l\neq k}$, Rabi frequency Ω_l, laser

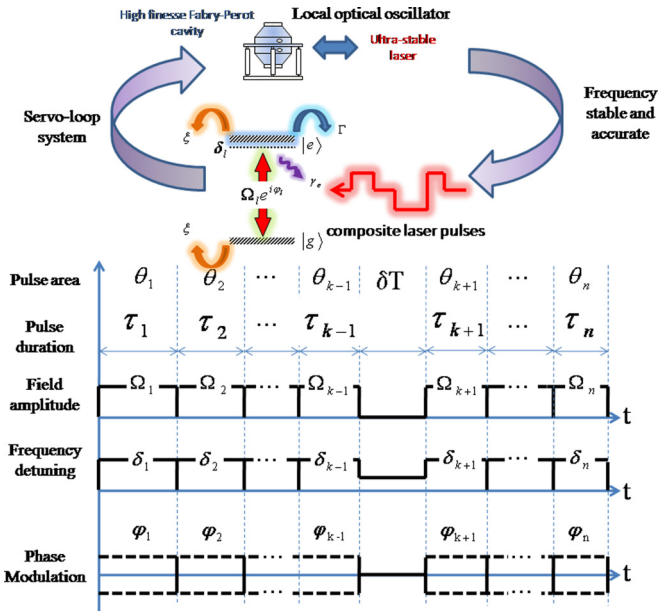

FIG. 1. Composite laser pulse spectroscopy probing a fermionic or a bosonic clock transition perturbed by dissipative processes. Optical pulses are defined by a generalized area θ_l ($l = 1,2,\ldots,k,\ldots,n$), the frequency detuning δ_l, the field amplitude $\Omega_l e^{i\varphi_l}$ including a phase-step modulation φ_l, a pulse duration τ_l, and a single free evolution time T applied somewhere at the desired $l = k$ pulse. The general clock frequency detuning is defined by $\delta_l = \delta - \Delta_l$ where a residual error in precompensation of laser-probe-induced frequency shift is Δ_l. The laser-induced decoherence is called γ_c, relaxation by spontaneous emission is labeled Γ, and ξ is the relaxation rate of the population difference due to collisions.

detuning δ_l, and phase φ_l of the coherent electromagnetic field can be modified independently over the entire sequence. The general set of time-dependent optical Bloch equations for a two-level $\{|g\rangle,|e\rangle\}$ quantum system for the lth pulse is given by [41–46]

$$\begin{aligned}\dot{U}_l &= -\gamma_c U_l + \delta_l V_l - \Omega_l \sin\varphi_l W_l,\\ \dot{V}_l &= -\delta_l U_l - \gamma_c V_l + \Omega_l \cos\varphi_l W_l,\\ \dot{W}_l &= \Omega_l \sin\varphi_l U_l - \Omega_l \cos\varphi_l V_l - (\Gamma + 2\xi) W_l - \Gamma,\end{aligned} \tag{1}$$

where $\delta_l = \delta - \Delta_l$ is the generalized clock frequency detuning, with δ being the laser frequency detuning from the unperturbed clock resonance. A frequency offset is added to the detuning δ during all light pulses, but not during the free evolution time T, to bring back the observed central fringe near $\delta = 0$ [25]. Δ_l is the part of the frequency shift not compensated by the applied frequency offset. Optical coherence and population difference are related to density matrix elements by $U_l \equiv \rho_{ge} + \rho_{ge}^*$, $V_l \equiv i(\rho_{ge} - \rho_{ge}^*)$, and $W_l \equiv \rho_{ee} - \rho_{gg}$. Population conservation is given by the relation $\rho_{gg} + \rho_{ee} = 1$. The complete three-vector components $M(\theta_l) \equiv (U(\theta_l), V(\theta_l), W(\theta_l))$ solution to the previous set of equations is [42,44]

$$M(\theta_l) = R(\theta_l)[M_l(0) - M_l(\infty)] + M_l(\infty), \tag{2}$$

where we introduce for convenience a generalized pulse area $\theta_l = \omega_l \tau_l$ and a generalized Rabi frequency ω_l (see

Appendix A for all definitions). The rotation matrix $R(\theta_l)$, taking into account decoherence and relaxation terms, is written as follows:

$$R(\theta_l) = e^{-\gamma_c \tau_l} e^{-\beta_l \tau_l},$$
$$\beta_l = \begin{pmatrix} 0 & \delta & -\Omega_l \sin\varphi_l \\ -\delta & 0 & \Omega_l \cos\varphi_l \\ \Omega_l \sin\varphi_l & -\Omega_l \cos\varphi_l & \Delta\gamma \end{pmatrix}, \quad (3)$$

with $\Delta\gamma = \gamma_c - (\Gamma + 2\xi)$. $M_l(0) \equiv (U_l(0), V_l(0), W_l(0))$ stands for the system's state before the lth pulse. The exponential matrix $R(\theta_l)$ can be exactly expressed as a square matrix of time-dependent matrix elements $R_{mn}(\theta_l)$ $(m,n = 1,2,3)$ (refer to Appendix A for all details). Steady-state solutions $M_l(\infty) \equiv (U_l(\infty), V_l(\infty), W_l(\infty))$ are directly obtained by switching off time-dependent derivatives in Eq. (1) for the three vector components. The free evolution matrix $R(\theta_k)$ at index $l = k$ without laser field reduces to

$$R(\theta_k = \delta T) = e^{-\gamma_c T} \begin{pmatrix} \cos\delta T & \sin\delta T & 0 \\ -\sin\delta T & \cos\delta T & 0 \\ 0 & 0 & e^{\Delta\gamma T} \end{pmatrix}. \quad (4)$$

The corresponding stationary solution $M_k(\infty) \equiv (U_k(\infty), V_k(\infty), W_k(\infty))$ is also found by switching off the laser field $\Omega_k = 0$ in Eq. (1) during free evolution time.

The complete solution of Bloch-vector components for a full sequence can ultimately be expressed in a reduced canonical form:

$$M(\theta_1, \ldots, \theta_n) \equiv A + B(\Phi)\cos(\delta T + \Phi), \quad (5)$$

which is the generalization to n pulses of the expression established for $n = 3$ [33]. The offset term A is given by

$$A = \sum_{p=k+1}^{n} \left[\left(\prod_{l=p}^{\overleftarrow{n}} R(\theta_l) \right) [M_{p-1}(\infty) - M_p(\infty)] \right] + M_n(\infty) + h e^{-(\Gamma+2\xi)T} \begin{pmatrix} \tilde{R}_{13} \\ \tilde{R}_{23} \\ \tilde{R}_{33} \end{pmatrix}. \quad (6)$$

The amplitude term $B(\Phi)$ components are given by

$$B_i(\Phi_i) = e^{-\gamma_c T} |C_i| \sqrt{1 + \tan^2 \Phi_i} \quad i \in \{1,2,3\}, \quad (7)$$

and the phase-shift term Φ components are written as

$$\Phi_i = -\arctan[S_i/C_i]\, i \in \{1,2,3\},$$
$$S \equiv \begin{pmatrix} \tilde{R}_{11} g - \tilde{R}_{12} f \\ \tilde{R}_{21} g - \tilde{R}_{22} f \\ \tilde{R}_{31} g - \tilde{R}_{32} f \end{pmatrix}, \quad C \equiv \begin{pmatrix} \tilde{R}_{11} f + \tilde{R}_{12} g \\ \tilde{R}_{21} f + \tilde{R}_{22} g \\ \tilde{R}_{31} f + \tilde{R}_{32} g \end{pmatrix}, \quad (8)$$

where $\tilde{R}_{mn}$ $(m,n = 1,2,3)$ are the matrix elements of the compiled matrix $\tilde{R}$ and (f,g,h) components are given by

$$\tilde{R} = \prod_{l=k+1}^{\overleftarrow{n}} R(\theta_l),$$
$$\begin{pmatrix} f \\ g \\ h \end{pmatrix} = \sum_{p=1}^{k} \left(\prod_{l=p}^{\overleftarrow{k-1}} R(\theta_l) \right) [M_{p-1}(\infty) - M_p(\infty)], \quad (9)$$

TABLE I. Composite laser-pulses interrogation protocols ignoring dissipative processes. The clock frequency shift including residual error in precompensation of probe-induced frequency shifts Δ is given by $\delta\tilde{\nu}(\Delta/\Omega)$. Pulse area $\boldsymbol{\theta_l}$ is given in degrees and phase steps $\varphi_{l+}, \varphi_{l-}$ are indicated in subscript parentheses in units of radians. The standard Rabi frequency for all pulses is $\Omega = \pi/2\tau$ where τ is the pulse duration reference. Free evolution appears at index $k = 2$, denoted $\theta_k = \delta T$. Reverse composite pulses protocols are denoted by (†).

Protocol [Ref.]	Composite pulses $\boldsymbol{\theta_{l(\varphi_{l+},\varphi_{l-})}}$	$\delta\tilde{\nu}(\Delta/\Omega)$
R [24]	$\mathbf{90}_{(\frac{\pi}{2},-\frac{\pi}{2})} \dashv \delta T \vdash \mathbf{90}_{(0,0)}$ $(\dagger)\mathbf{90}_{(0,0)} \dashv \delta T \vdash \mathbf{90}_{(-\frac{\pi}{2},\frac{\pi}{2})}$	$\frac{1}{\pi T}\frac{\Delta}{\Omega}$
HR [32,33]	$\mathbf{90}_{(\frac{\pi}{2},-\frac{\pi}{2})} \dashv \delta T \vdash \mathbf{180}_{(\pi,\pi)}\mathbf{90}_{(0,0)}$ $(\dagger)\mathbf{90}_{(0,0)}\mathbf{180}_{(\pi,\pi)} \dashv \delta T \vdash \mathbf{90}_{(-\frac{\pi}{2},\frac{\pi}{2})}$	$\frac{4}{\pi T}\left(\frac{\Delta}{\Omega}\right)^3$
MHR [37]	$\mathbf{90}_{(\frac{\pi}{2},0)} \dashv \delta T \vdash \mathbf{180}_{(\pi,\pi)}\mathbf{90}_{(0,-\frac{\pi}{2})}$ $(\dagger)\mathbf{90}_{(-\frac{\pi}{2},0)}\mathbf{180}_{(\pi,\pi)} \dashv \delta T \vdash \mathbf{90}_{(0,\frac{\pi}{2})}$	0
GHR($\frac{\pi}{4}$) [34]	$\mathbf{90}_{(0,0)} \dashv \delta T \vdash \mathbf{180}_{(\frac{\pi}{4},-\frac{\pi}{4})}\mathbf{90}_{(0,0)}$ $(\dagger)\mathbf{90}_{(0,0)}\mathbf{180}_{(-\frac{\pi}{4},\frac{\pi}{4})} \dashv \delta T \vdash \mathbf{90}_{(0,0)}$	0
GHR($\frac{3\pi}{4}$) [34]	$\mathbf{90}_{(0,0)} \dashv \delta T \vdash \mathbf{180}_{(3\frac{\pi}{4},-3\frac{\pi}{4})}\mathbf{90}_{(0,0)}$ $(\dagger)\mathbf{90}_{(0,0)}\mathbf{180}_{(-\frac{3\pi}{4},\frac{3\pi}{4})} \dashv \delta T \vdash \mathbf{90}_{(0,0)}$	0

where backward arrows indicate a matrix product from right to left with growing indices. The generalized hyper-Ramsey canonical expression describing the population transfer from $|g\rangle$ to $|e\rangle$ clock states is given by the third component of the Bloch variables. Various composite pulse protocols and their time-reversed counterparts reported in Table I can be simulated using Eq. (5).

A high-order expression of the clock frequency shift $\delta\nu \approx -\Phi|_{\delta\to 0}/2\pi T$ affecting the extremum of the central fringe pattern of the GHR resonance from Eq. (5) is presented in Appendix B. Ignoring dissipative processes, analytical expressions have already been derived for Ramsey and hyper-Ramsey protocols in Refs. [33,35]. The typical nonlinear response of a GHR resonance line shape to probe-induced frequency shifts is usually asymmetric leading to off-center line locking when a laser frequency modulation technique is applied. In the next section, we present the phase-step modulation of the resonance shape which eliminates the effect of that asymmetry on the true position of the central fringe.

III. ERROR SIGNAL GENERATION WITH PHASE-MODULATED (GHR) RESONANCE

A laser frequency stabilization scheme based on antisymmetric laser phase steps is able to synthesize a dispersive error signal locking the laser frequency to the center of the perturbed clock transition [29,31]. This technique is applied by measuring experimentally the population transfer $P_{|g\rangle\mapsto|e\rangle}$ between clock states. The phase-modulated Ramsey scheme requires the relative phase of the second optical Ramsey pulse to be shifted by $\pm\pi/2$ with respect to the first pulse.

For simplicity, we now focus on the third Bloch variable component related to population difference and we will omit indices in subsequent expressions. The error signal ΔE for a particular protocol is built by taking the difference between two Bloch-vector components $M(\theta_1, \ldots, \theta_n)$ with appropriate

phase-steps modulation $_{(\varphi_{l+},\varphi_{l-})}$ of a specified pulse area θ_l. The resulting line shape for population transfer between clock states is

$$\begin{aligned}\Delta E &\equiv M(\theta_1,\ldots,\theta_n)(\varphi_{l+}) - M(\theta_1,\ldots,\theta_n)(\varphi_{l-}) \\ &= [P_{|g\rangle\mapsto|e\rangle}(\varphi_{l+}) - P_{|g\rangle\mapsto|e\rangle}(\varphi_{l-})]. \end{aligned} \tag{10}$$

The new phase-modulated line shape can also be rewritten in yet another phasor canonical form as

$$\Delta E \equiv \tilde{A} + \tilde{B}(\tilde{\Phi})\cos(\delta T + \tilde{\Phi}), \tag{11}$$

where offset $\tilde{A}$, amplitude $\tilde{B}$, and phase shift $\tilde{\Phi}$ are explicitly given in Appendix C. The error signal shape for the third component related to the population difference exhibits a dispersive feature versus clock frequency detuning, unlike the GHR resonance curve [33]. From the condition $\Delta E|_{\delta=\delta\widetilde{\nu}} = 0$ due to imperfect probe-induced frequency shift compensation, it is straightforward to derive an analytical form of the frequency-shifted locking point $\delta\widetilde{\nu}$ as

$$\delta\widetilde{\nu} = \frac{1}{2\pi T}\left(-\tilde{\Phi}|_{\delta\to 0} \pm \arccos\left[-\frac{\tilde{A}|_{\delta\to 0}}{\tilde{B}(\tilde{\Phi})|_{\delta\to 0}}\right]\right). \tag{12}$$

The robustness of various error signals to a modification of pulse area and uncompensated frequency shifts has already been numerically studied in detail when decoherence is non-negligible [38]. The fundamental consequence for all optical interrogation schemes is a rapid loss of the laser frequency locking-point stability inducing, for example, additional constraints concerning the MHR protocol [38]. To explore in more depth the instability of frequency locking points caused by dissipative processes, clock frequency shifts for various interrogation protocols have been extracted from general offset and amplitude terms established in the previous section, Eq. (11) and Eq. (12). They are investigated with the help of 2D contour and density plot diagrams presented in the next section.

IV. 2D DIAGRAMS FOR CLOCK FREQUENCY SHIFT RECONSTRUCTION

The influence of decoherence or relaxation by spontaneous emission on HR and GHR probing schemes is analyzed using 2D contour and density plot diagrams shown in Figs. 2 and 3. All clock-frequency shifts $\delta\widetilde{\nu}$ are plotted using Eq. (12) versus uncompensated frequency shifts and large pulse area variations. Because ac Stark shifts increasing quadratically with pulse area might still be manageable by applying a larger laser frequency step for precompensation of the central fringe frequency shift [25], diagrams are also exploring regions of several $\pi/2$ laser pulse area units. Note that the error signal contrast is always maximized for odd values of multiples of $\Omega\tau = \pi/2$ pulses and vanishing for even values. Colored values of clock-frequency shifts have been deliberately limited between -2 mHz and $+2$ mHz for constraint below 10^{-18} relative accuracy. The white background represents some regions where the residual shift exceeds a few 10^{-18} levels of relative accuracy.

The dependence of the HR error signal ΔE[HR] on uncontrollable modifications of laser parameters, ignoring dissipative processes, is presented in Figs. 2(a1) and 2(a2). The 2D contour and density plots exhibit some stable regions where the third-order dependence of the clock shift $\delta\widetilde{\nu}$[HR] is well below 500 μHz over 100 mHz of uncompensated frequency shifts (pink and violet region along the vertical axis). The clock-frequency-shift compensation can be made more robust over a wider range of residual frequency shifts by increasing the pulse area from $\pi/2$ to a magic value near $2.95\pi/2$ as shown in Fig. 2(a2). At this particular value, all contour plots (black thin isoclinic lines delimiting regions) present vanishing first-order derivative versus pulse area variation making the frequency locking point even more stable to small laser power modification. Noteworthy frequency locking points are also observed near the value of $1.2\pi/2$ or near $2.6\pi/2$. Around these values, the clock frequency shift is changing abruptly from positive to negative values for small errors in compensation of probe-induced frequency shifts. When there is decoherence, a modification of the $\delta\widetilde{\nu}$[HR] clock-frequency shift is observed in Figs. 2(b1), 2(b2) leading to a linear increase of the shift up to 2 mHz over 100 mHz of uncompensated frequency shifts. However, a small frequency stability island (small pink and violet region) emerges in Fig. 2(b2) for a pulse area near $\sim 3.25\pi/2$. When decoherence and relaxation by spontaneous emission are both present as shown in Figs. 2(c1), 2(c2), the clock frequency shift is reversed with a negative slope of 2 mHz over 400 mHz of uncompensated frequency shifts.

We have also studied the influence of decoherence on Eq. (12) with GHR($\pi/4$) and GHR($3\pi/4$) protocols presented in Table I. Clock frequency shift $\delta\widetilde{\nu}$[GHR($\pi/4$)] and $\delta\widetilde{\nu}$[GHR($3\pi/4$)] responses to laser parameter modifications are reported in 2D contour and density plot diagrams in Figs. 3(a1), 3(a2) and 3(b1), 3(b2). It is worthwhile to note that if decoherence is vanishing, GHR($\pi/4$) and GHR($3\pi/4$) are indeed very efficient and lead to a complete suppression of probe-induced frequency shifts $\delta\widetilde{\nu} = 0$ at all orders (see Table I). This is why the figure equivalent to Figs. 2(a1), 2(a2) is not shown. If the laser linewidth is not negligible, generating decoherence γ_c, robustness of GHR protocols to laser power variation and uncompensated frequency shifts are strongly degraded leading to Fig. 3. The radiative case $\Gamma \neq 0$ leads to an important increase of clock frequency shifts $\delta\widetilde{\nu}$[GHR($\pi/4$)] and $\delta\widetilde{\nu}$[GHR($3\pi/4$)] and is not considered here.

The simultaneous observation of Figs. 3(a2) and 3(b2) shows that frequency locking-point regions of instability marked by different colored density plots are of opposite sign. It is thus possible to reconstruct another synthetic frequency shift $\delta\widetilde{\nu}$[syn] to reliably suppress probe-induced shifts and their variations for GHR($\pi/4$) and GHR($3\pi/4$) interrogation schemes. Taking the half sum of the two clock frequency shifts $\delta\widetilde{\nu}$[GHR($\pi/4$)] and $\delta\widetilde{\nu}$[GHR($3\pi/4$)] shown in Figs. 3(c1), 3(c2) displays small frequency locking-point stability islands near the $\pi/2$ and $3\pi/2$ pulse area (pink and violet regions along the horizontal axis). This synthetic residual frequency shift becomes much less sensitive to variations in laser power and probe shifts [38].

2D diagrams help in generating some stable regions by combining frequency-shift measurements when dissipative processes are present, but the process requires a post-data treatment and the synthetic laser frequency locking point is never absolutely protected against residual probe shifts and laser power variations degrading the clock stability.

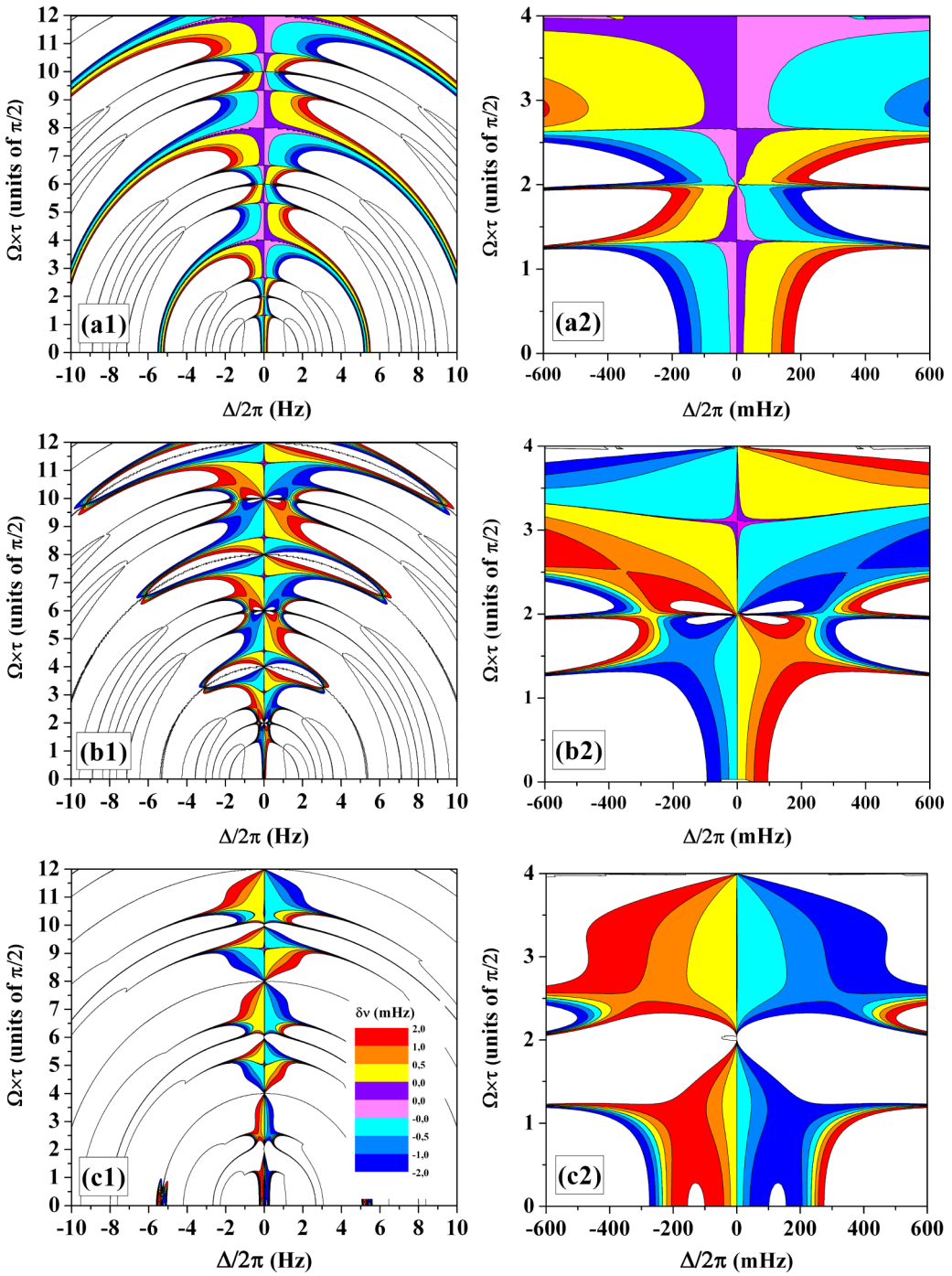

FIG. 2. 2D contour and density plot diagrams of the $\delta\widetilde{\nu}$[HR] clock frequency shift based on Eq. (12) versus uncompensated frequency shifts $\Delta/2\pi$ (horizontal axis) and pulse area variation $\Omega\tau$ (vertical axis). Left graphs are over a large detuning acceptance bandwidth and right graphs are expanded between $\pi/2$ and $3\pi/2$ pulse areas. (a1), (a2) Ideal case. (b1), (b2) Decoherence $\gamma_c = 2\pi \times 50$ mHz. (c1), (c2) Decoherence and relaxation $\gamma_c = 2\pi \times 50$ mHz, $\Gamma = 2\pi \times 100$ mHz. The standard Rabi frequency for all pulses is $\Omega = \pi/2\tau$ where τ is the pulse duration reference. Pulse duration reference is set to $\tau = 3/16$ s, free evolution time is $T = 2$ s, and uncompensated frequency shift is $\Delta_l \equiv \Delta$ ($l = 1,3,4$).

V. UNIVERSAL ELIMINATION PROTOCOL OF PROBE-FIELD-INDUCED FREQUENCY SHIFTS

Although a recent frequency-shift extrapolation-based method based on multiple (HR) schemes with different free evolution times was proposed to reduce imperfect compensation of probe-induced shifts well below a fractional frequency change of 10^{-18} [38], the existence of an absolute interrogation protocol directly canceling these shifts on the dispersive error signal shape at all orders even in presence of decoherence, relaxation by spontaneous emission, and collisions has not yet been established.

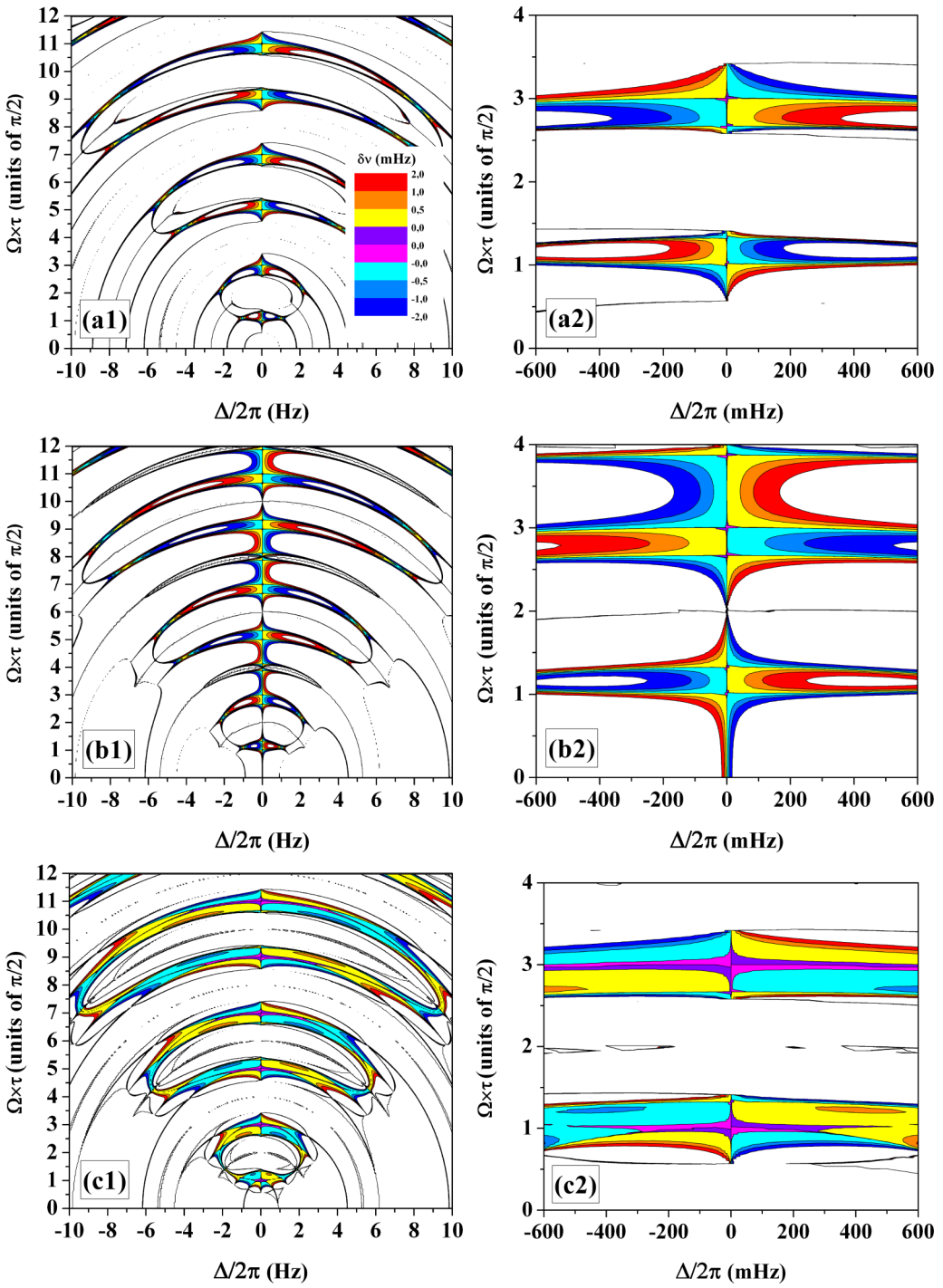

FIG. 3. 2D contour and density plot diagrams of the $\delta\widetilde{\nu}$[GHR($\pi/4$)] and $\delta\widetilde{\nu}$[GHR($3\pi/4$)] clock frequency shifts based on Eq. (12) under decoherence $\gamma_c = 2\pi \times 50$ mHz versus uncompensated frequency shifts $\Delta/2\pi$ (horizontal axis) and pulse area variation $\Omega\tau$ (vertical axis). Left graphs are over a large detuning acceptance bandwidth and right graphs are expanded between $\pi/2$ and $3\pi/2$ pulse areas. (a1), (a2) $\delta\widetilde{\nu}$[GHR($\pi/4$)] diagram. (b1), (b2) $\delta\widetilde{\nu}$[GHR($3\pi/4$)] diagram. (c1), (c2) Synthetic frequency shift $\delta\widetilde{\nu}$[syn] $= \frac{1}{2}\{\delta\widetilde{\nu}$[GHR($\pi/4$)] + $\delta\widetilde{\nu}$[GHR($3\pi/4$)]$\}$. Other parameters are identical to Fig. 2.

To solve the problem, we propose in Fig. 4 a universal interrogation protocol denoted GHR($\pi/4, 3\pi/4$) based on mixing GHR($\pi/4$) and GHR($3\pi/4$) schemes from Table I, interleaved or not by a controllable population inversion between clock states. Symmetric properties of the interrogation scheme might be even exploited with some quantum logic gate circuits using entanglement of prepared qubits [47], reducing the number of measurements required to generate the correct laser frequency locking point. Unlike the synthetic frequency-shift realization presented in Fig. 3(c2) which requires combining two separated clock frequency shift evaluations potentially degrading the clock stability, our universal protocol generates

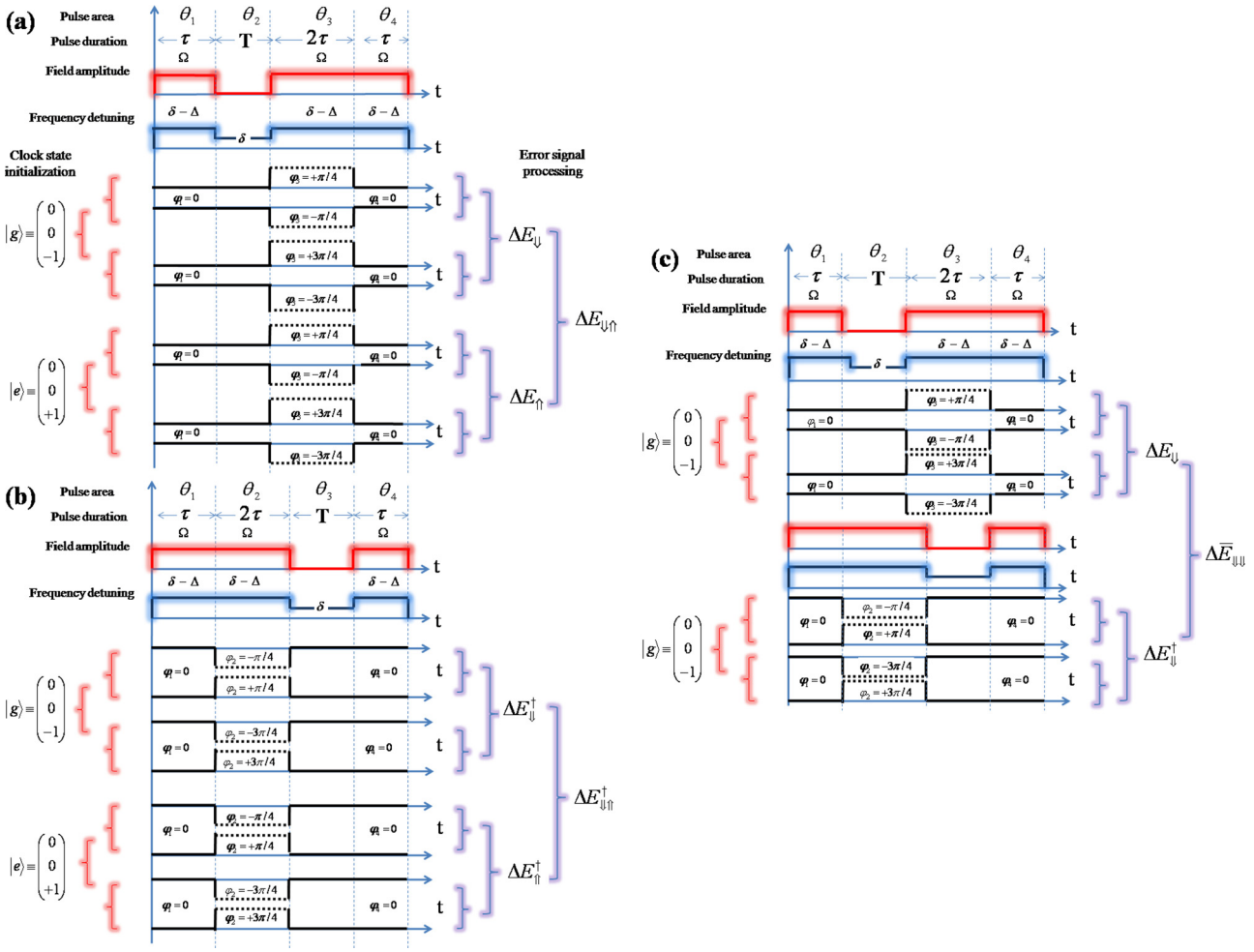

FIG. 4. Universal laser frequency interrogation schemes for ultrarobust frequency locking points based on a combination of error signals generated by GHR($\pi/4$) and GHR($3\pi/4$) protocols from Table. I. (a) Interrogation protocol including a controllable population inversion between clock states. (b) Equivalent mirror-like interrogation protocol obtained by applying the transformation $t \to -t$ and $\varphi \to -\varphi$ on the scheme from (a). (c) Synthetic universal interrogation protocol by combining parts of (a) and (b) schemes, which eliminates population initialization in the upper state.

a direct laser frequency locking point as a strong error signal gradient robust even to substantial uncompensated frequency shifts.

The universal interrogation protocol GHR($\pi/4,3\pi/4$) breaks down into three different layouts of composite optical pulses as shown in Figs. 4(a)–4(c). The initial combination of GHR($\pi/4$) and GHR($3\pi/4$) protocols from Table I, presented in Fig. 4(a), includes a population inversion between clock states. Phase steps are applied only during the third pulse interaction following a free evolution time. A similar interrogation scheme can be realized using reverse composite pulses as in Fig. 4(b) with mirror-like protocols denoted by † type from Table I. In such a case, while ignoring stationary states, a time and phase reversal symmetry transformation can be applied on the scheme presented in Fig. 4(a) to recover an identical line shape obtained with Fig. 4(b) and mirror-like protocol [33]. A new frequency locking point can still be synthesized as shown in Fig. 4(c) mixing some parts of the two previous protocols while eliminating population initialization in the upper state. Such an alternative scheme might be seen as a sort of spin echo hybrid technique [48] removing some uncontrollable variations of laser parameters with time order pulse reversal. In all cases, the new error signal $\Delta E[\mathrm{GHR}(\pi/4,3\pi/4)]$ requires a specific number of atomic population fraction measurements to generate a robust laser frequency locking point depending on the nature of the dissipative processes impacting the atomic transition. The ideal laser frequency locking point with no correction for uncompensated probe induced frequency shifts is provided by the use of $\pm\pi/4$ and $\pm 3\pi/4$ phase steps which cancel exactly steady-state solutions from Bloch solutions [see for example Eq. (D2) in Appendix D].

When an ideal two-level system is considered, error signals based on MHR and GHR protocols require only 2 population fraction measurements generating a very stable frequency locking point with full elimination of residual clock frequency shifts $\delta\widetilde{\nu}$ as reported in Table I. For a pure decoherence case affecting the frequency locking point stability as shown in Fig. 3(a2) and Fig. 3(b2), a combination of 4 atomic population fraction measurements with $\pm\pi/4$ and $\pm 3\pi/4$ phase steps and one single state initialization [half part of the universal protocol from Fig. 4(a) or Fig. 4(b) called † type] is sufficient to totally cancel the probe-induced frequency shifts. The normalized

error signal denoted $\Delta E_{\Downarrow(\Uparrow)} \equiv \Delta E[\mathrm{GHR}(\pi/4,3\pi/4)]$ (or equivalently † type) is generated as follows:

$$\begin{aligned}\Delta E_{\Downarrow(\Uparrow)} &= \tfrac{1}{2}\{\Delta E[\mathrm{GHR}(\pi/4)]-\Delta E[\mathrm{GHR}(3\pi/4)]\}_{\Downarrow(\Uparrow)},\\ \Delta E^{\dagger}_{\Downarrow(\Uparrow)} &= \tfrac{1}{2}\{\Delta E^{\dagger}[\mathrm{GHR}(\pi/4)]-\Delta E^{\dagger}[\mathrm{GHR}(3\pi/4)]\}_{\Downarrow(\Uparrow)},\end{aligned} \tag{13}$$

where $\Downarrow$ ($\Uparrow$) means the protocol is applied with population initialization in either ground state $|g\rangle \equiv \Downarrow$ or excited state $|e\rangle \equiv \Uparrow$.

For simultaneous activation of spontaneous emission and decoherence, the error signal thus requires 8 atomic population measurements divided into 4 measurements with state initialization in $|g\rangle$ and $|e\rangle$ [see Fig. 4(a)]. The dispersive error signal $\Delta E_{\Downarrow\Uparrow} \equiv \Delta E[\mathrm{GHR}(\pi/4,3\pi/4)]$ ($\Delta E^{\dagger}_{\Downarrow\Uparrow}$) now becomes

$$\begin{aligned}\Delta E_{\Downarrow\Uparrow} &= \tfrac{1}{2}(\Delta E_{\Downarrow} - \Delta E_{\Uparrow}) = F_{\Downarrow\Uparrow}[M(0),\theta_1,\theta_3]\sin(\delta T),\\ \Delta E^{\dagger}_{\Downarrow\Uparrow} &= \tfrac{1}{2}(\Delta E^{\dagger}_{\Downarrow} - \Delta E^{\dagger}_{\Uparrow}) = F^{\dagger}_{\Downarrow\Uparrow}[M(0),\theta_1,\theta_3]\sin(\delta T),\end{aligned} \tag{14}$$

where amplitude functions $F[M(0),\theta_1,\theta_3]$ can be derived from Appendix D.

Note that an additional protocol presented in Fig. 4(c) can synthesize another ultrastable frequency locking point while avoiding population initialization in both quantum states. We apply now a linear combination of error signals from two

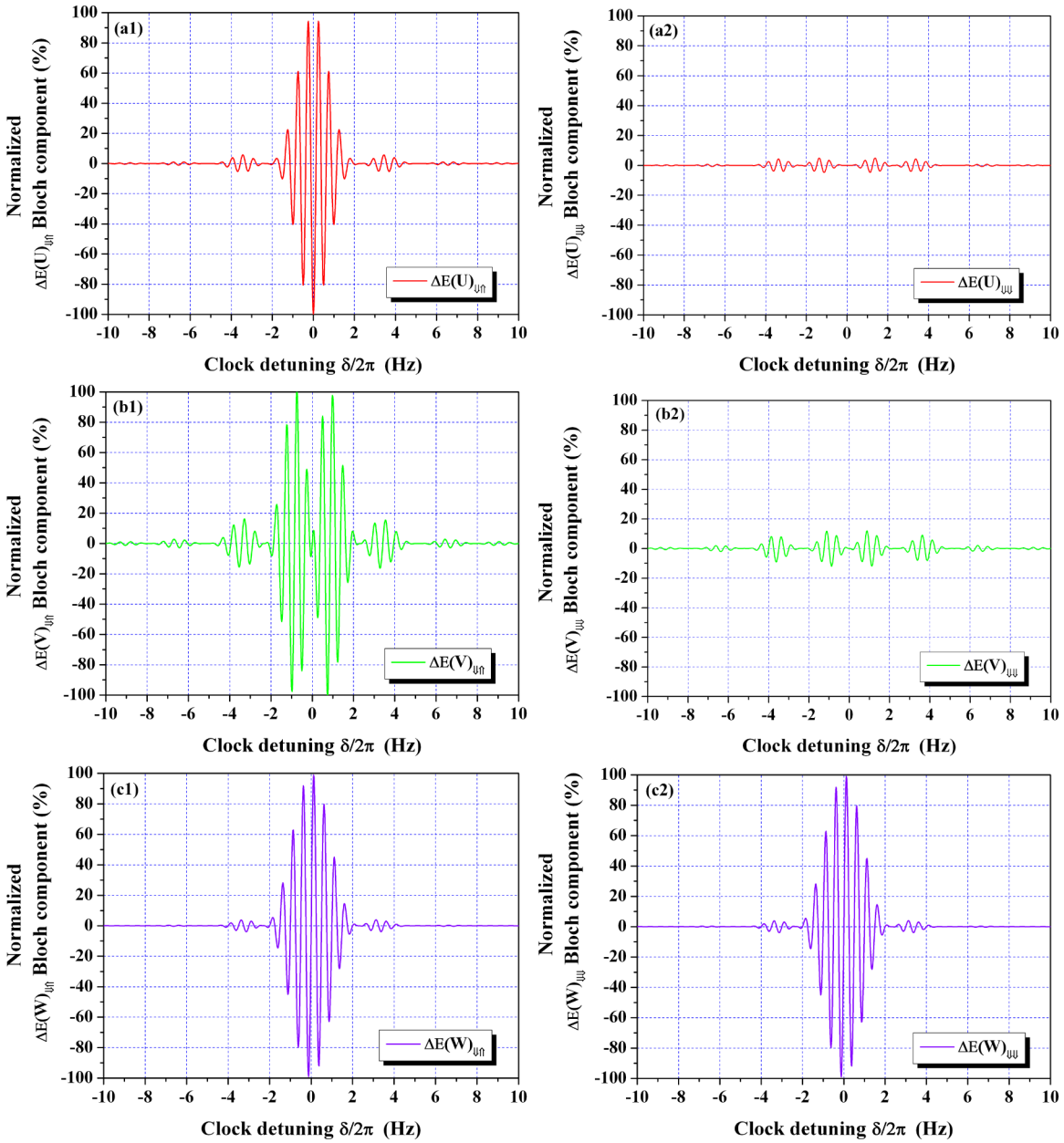

FIG. 5. Comparison of normalized line shapes and signal amplitudes of the three-Bloch-vector component (U,V,W) versus clock frequency detuning $\delta/2\pi$ for protocols $\Delta E_{\Downarrow\Uparrow}$ of Figs. 4(a), 4(b) (left panels) and $\Delta\overline{E}_{\Downarrow\Downarrow}$ of Fig. 4(c) (right panels). (a1) Bloch component $\Delta E(U)_{\Downarrow\Uparrow}$ and (a2) $\Delta\overline{E}(U)_{\Downarrow\Downarrow}$. (b1) Bloch component $\Delta E(V)_{\Downarrow\Uparrow}$ and (b2) $\Delta\overline{E}(V)_{\Downarrow\Downarrow}$. (c1) Bloch component $\Delta E(W)_{\Downarrow\Uparrow}$ and (c2) $\Delta\overline{E}(W)_{\Downarrow\Downarrow}$. The standard Rabi frequency for all pulses is $\Omega = \pi/2\tau$ where τ is the pulse duration reference. Pulse duration is $\tau = 3/16$ s with free evolution time $T = 2$ s. We have ignored probe-induced frequency shifts and dissipative processes for comparison between amplitude curves.

opposite sequences of composite laser pulses that are reversed in time ordering as

$$\Delta\overline{E}_{\Downarrow\Downarrow} = \tfrac{1}{4}(\Delta E^{\dagger}_{\Downarrow} + \Delta E_{\Downarrow}) = F_{\Downarrow\Downarrow}[M(0),\theta_1,\theta_3]\sin(\delta T), \tag{15}$$

where amplitude function $F[M(0),\theta_1,\theta_3]$ can be derived from Appendix E. Note that such an error signal $\Delta\overline{E}_{\Downarrow\Downarrow}$ is remarkable over a few additional features. It produces a zero crossing point with enhanced immunity to residual offset variations independent of a perfect quantum state initialization.

We have reported all Bloch-vector component error signal line shapes with normalized amplitudes for $\Delta E_{\Downarrow\Uparrow}$ and $\Delta E_{\Downarrow\Downarrow}$ in Fig. 5 ignoring dissipative processes. Curves from the right panels are normalized respectively to the ones from left panels showing very different signal strengths in real and imaginary parts of the optical coherence under identical choice of laser parameters. Notice that if a simultaneous laser probe transmission monitoring is allowed with the first universal protocol $\Delta E_{\Downarrow\Uparrow}$, a parallel implementation of a feedback loop control may be realized by recording imaginary and real parts of the optical coherence [see Eq. (D5) in Appendix D and Figs. 5(a1), 5(b1)] as an additional hint signal to steer any probe frequency drift in the correct direction over long periods of time. The second universal protocol $\Delta E_{\Downarrow\Downarrow}$ does even not require any elimination of residual optical coherence after the entire interrogation process because nonvanishing real and imaginary parts of any optical coherence, which may interfere with the laser probe during the pulse spectroscopy [49], are exhibiting the same dispersive line shape locked at the unperturbed clock frequency [see Eq. (E2) in Appendix E].

We have respectively reported in Figs. 6(a)–6(a) typical error signal patterns ΔE[HR], ΔE[MHR], and $\Delta E_{\Downarrow\Uparrow}$ versus the clock detuning under simultaneous action of decoherence and relaxation. It is clearly demonstrated that the laser frequency locking point generated by $\Delta E_{\Downarrow\Uparrow}$ is ultrarobust against dissipation and residual uncompensated probe-induced frequency shifts compared to other schemes. The robustness of the normalized error signal slope to uncompensated frequency shifts and pulse area variation is presented in Fig. 7(a). The $\Delta E_{\Downarrow\Uparrow}$ ($\Delta E^{\dagger}_{\Downarrow\Uparrow}$) acceptance bandwidth is two times larger than the ΔE[HR] error signal under identical laser parameters. A very large $\pm 10\%$ error on the laser field amplitude slightly modifies the slope but does not degrade the frequency locking range where the slope does not drop to zero. We have also checked that all universal interrogation schemes do not need to rely on a perfect 100% initialization of the excited state. Investigating various analytical $\Delta E_{\Downarrow\Uparrow}$ ($\Delta E^{\dagger}_{\Downarrow\Uparrow}$) error signal shape expressions (see Appendix D), nonideal population inversion between quantum states, for example due to large frequency shifts induced by a π pulse excitation, will lead only to a linear reduction in size amplitude of the generated error signal with no deterioration of the laser frequency locking point robustness.

We finally report in Fig. 7(b) the sensitivity of $\delta\widetilde{\nu}$[HR] and $\delta\widetilde{\nu}[\Delta E_{\Downarrow\Uparrow}]$ clock frequency shifts to residual uncompensated probe shifts for pulse area variations of $\Delta\theta/\theta = \pm 10\%$ and various dissipative processes configurations already displayed. The $\delta\widetilde{\nu}$[HR] clock frequency shift measurement affecting the central fringe minimum for the HR protocol is shown

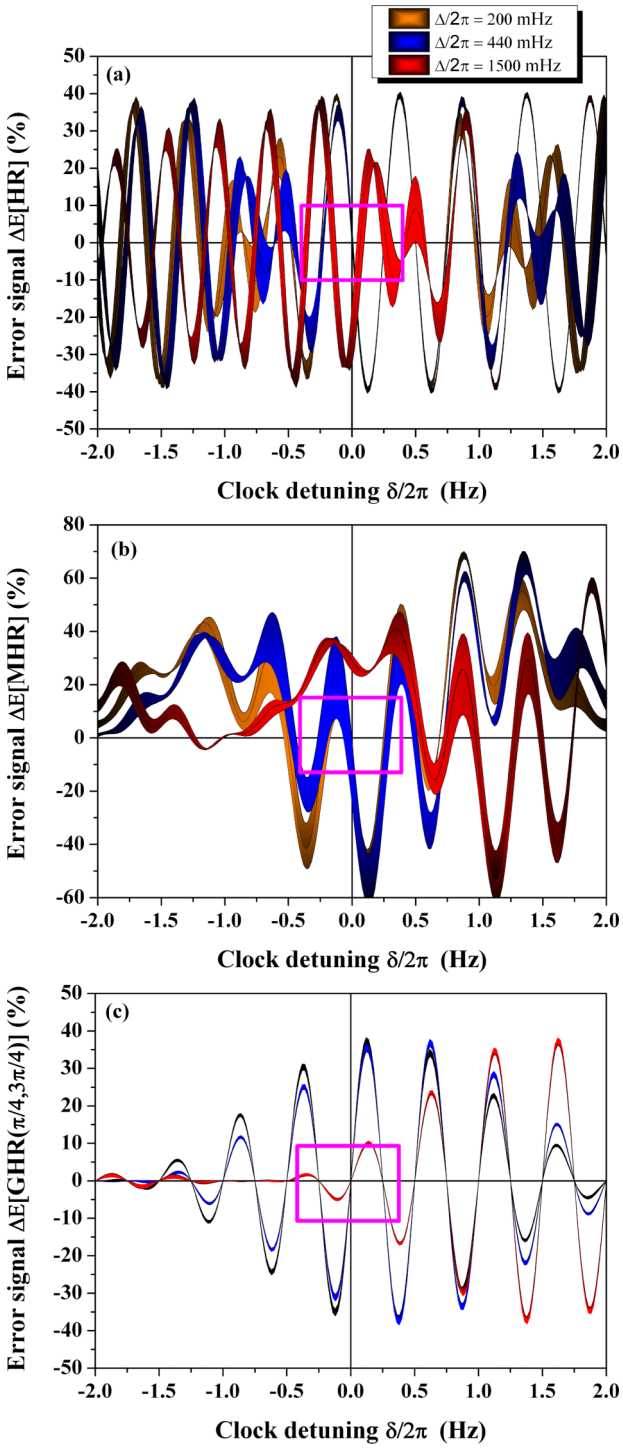

FIG. 6. Error signal shapes versus clock frequency detuning $\delta/2\pi$ for three different uncompensated frequency shifts $\Delta/2\pi$. The laser frequency locking point is delimited by a bounding box around $\delta \mapsto 0$. (a) ΔE[HR], (b) ΔE[MHR], and (c) $\Delta E_{\Downarrow\Uparrow}$. Resilience of the frequency locking point to various uncompensated probe-induced frequency shifts $\Delta/2\pi$ is demonstrated for the last scheme. Pulse area variation is set to $\Delta\theta/\theta = \pm 10\%$ (shadow regions). Dissipative parameters of the two-level system used as an atomic frequency reference are fixed to $\gamma_c = 2\pi \times 50$ mHz, $\Gamma = 2\pi \times 100$ mHz, and $\xi = 0$. The standard Rabi frequency for all pulses is $\Omega = \pi/2\tau$ where τ is the pulse duration reference. Pulse duration is $\tau = 3/16$ s with free evolution time $T = 2$ s.

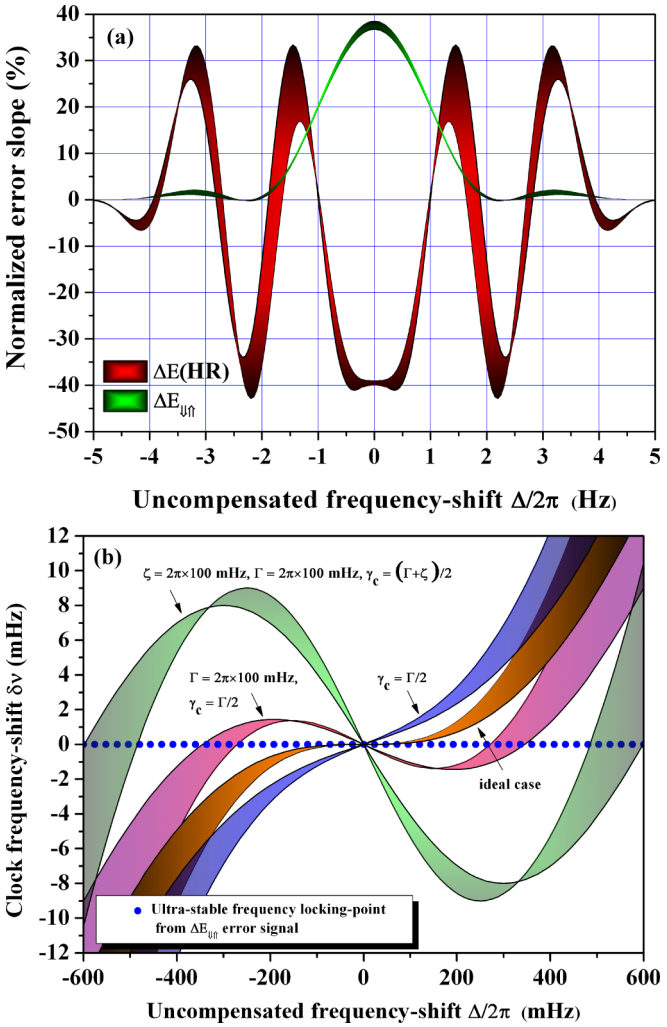

FIG. 7. Compared robustness of ΔE[HR] and $\Delta E_{\Downarrow\Uparrow}$ schemes with $\Delta\theta/\theta = \pm 10\%$ error in the laser field amplitude. (a) Acceptance bandwidth of normalized ΔE[HR] and $\Delta E_{\Downarrow\Uparrow}$ ($\Delta E^{\dagger}_{\Downarrow\Uparrow}$) error signal slopes versus uncompensated probe shifts $\Delta/2\pi$. (b) $\Delta E_{\Downarrow\Uparrow}$ (blue dots) and ΔE[HR] (solid line) clock frequency shifts when decoherence, relaxation by spontaneous emission, and collisions are toggled on-off. All other parameters are identical to Fig. 6.

in Fig. 7(b). It is worth noting the perfect cancellation of the locked frequency shift $\delta\widetilde{\nu}[\Delta E_{\Downarrow\Uparrow}]$ reported as blue dots, even in the presence of decoherence and relaxation. Table II summarizes absolute robustness of different error signal laser frequency locking points to various combinations of dissipative parameters γ_c, Γ, ξ, for a closed two-level system. Table III reports the ultimate clock frequency shift sensitivity from different error signal laser frequency locking points to a systematic error in the laser phase-stepping process by $\delta\varphi/\varphi = \pm 1\%$ under a strong pulse area variation by $\Delta\theta/\theta = \pm 10\%$ and for three different values of uncompensated frequency shifts. From this analysis, the ΔE[MHR] error signal presents a systematic parasitic shift even when a complete elimination of residual frequency shifts Δ is realized. The result is also consistent with a previous numerical work which was only for a pure decoherence effect [38]. Based on our complete GHR line-shape solution, we have been

TABLE II. Absolute robustness of various error signal laser frequency locking points to individual or multiple {} dissipative parameters γ_c, Γ, ξ for a closed two-level system. The number of atomic state population measurements N required to build the error signal is also indicated. A perfect phase stepping of the laser for all protocols is considered here. Note if $\Gamma \neq 0$, then $\gamma_c = \Gamma/2$ to be consistent with a pure radiative process.

Error signal	N	γ_c	ξ	$\{\gamma_c,\xi\}$	$\{\gamma_c,\Gamma\}$	$\{\gamma_c,\Gamma,\xi\}$
ΔE[HR] ΔE[GHR($\pi/4$)] ΔE[MHR] ΔE[GHR($3\pi/4$)]	2	NO	NO	NO	NO	NO
$\Delta E_{\Downarrow(\Uparrow)}$, $\Delta E^{\dagger}_{\Downarrow(\Uparrow)}$	4	✓	✓	✓	NO	NO
$\Delta E_{\Downarrow\Uparrow}$, $\Delta E^{\dagger}_{\Downarrow\Uparrow}$, $\Delta\overline{E}_{\Downarrow\Downarrow}$	8	✓	✓	✓	✓	✓

able to identify that the ΔE[HR] error signal also recovers a small parasitic shift due to a small imperfect phase-step modulation. We note that for uncompensated frequency shifts larger than $\Delta/2\pi \geqslant 1$ Hz, the HR slope has abruptly changed in sign as expected from Fig. 7(a) leading to a rapid loss of clock stability. However the larger acceptance bandwidth for universal schemes $\Delta\overline{E}_{\Downarrow\Downarrow}$ and $\Delta E_{\Downarrow\Uparrow}$ allows for maintaining a robust error signal gradient even for larger uncompensated probe-induced frequency shifts. They still ultimately suffer from a weak linear dependance to these uncompensated frequency shifts because a small error in phase steps breaks the perfect rejection of steady-state solutions when combining several atomic population fraction measurements.

VI. CONCLUSIONS

We have first established the analytical expression of the Bloch-vector evolution in the presence of decoherence and relaxation during a light pulse interaction. We then deduced the analytical equation of the Bloch-vector evolution of a two-level atom subjected to a series of light pulses of different lengths, laser detunings, field amplitudes, and phases. This allowed us to determine the error signal and shift of a probe laser frequency locked on a narrow optical transition biased by a probe-induced shift using various interrogating schemes, such as HR, MHR, or GHR techniques. It is shown that these techniques do not allow a full cancellation of the shift in the presence of dissipative processes. We have then proposed universal protocols based on composite pulses and $\pm\pi/4$ and

TABLE III. Estimation of various laser frequency locking-point frequency shifts $|\delta\widetilde{\nu}|$ (absolute value) to a systematic error in laser phase steps by $\delta\varphi/\varphi = \pm 1\%$. Dissipative atomic parameters are fixed to $\Gamma = 2\pi \times 100$ mHz and $\gamma_c = \Gamma/2$ under pulse area variation by $\Delta\theta/\theta = \pm 10\%$ for three residual uncompensated frequency shifts $\Delta/2\pi$. All frequency shifts are given in units of mHz.

Error signal	$\Delta/2\pi = 0$	$\Delta/2\pi = 440$	$\Delta/2\pi = 1500$
ΔE[MHR]	$\lvert\delta\widetilde{\nu}\rvert \leqslant 100$	$\lvert\delta\widetilde{\nu}\rvert \leqslant 100$	$\lvert\delta\widetilde{\nu}\rvert \leqslant 1000$
ΔE[HR]	$\lvert\delta\widetilde{\nu}\rvert \leqslant 10$	$\lvert\delta\widetilde{\nu}\rvert \leqslant 10$	out of range
$\Delta\overline{E}_{\Downarrow\Downarrow}$	$\lvert\delta\widetilde{\nu}\rvert = 0$	$\lvert\delta\widetilde{\nu}\rvert \leqslant 1$	$\lvert\delta\widetilde{\nu}\rvert \leqslant 10$
$\Delta E_{\Downarrow\Uparrow}$	$\lvert\delta\widetilde{\nu}\rvert = 0$	$\lvert\delta\widetilde{\nu}\rvert \leqslant 0.1$	$\lvert\delta\widetilde{\nu}\rvert \leqslant 1$

$\pm 3\pi/4$ phase modulation. The synthesized laser frequency locking point is absolutely robust against pulse area errors and uncompensated probe-induced frequency shifts in the presence of laser-induced decoherence and relaxation caused by both spontaneous emission and weak collisions. Here a composite laser-pulse interrogation protocol demonstrates a very efficient elimination of field-induced frequency shifts with noninteracting particles through large constraints in laser parameters. These schemes can be implemented in two flavors: either by inverting clock state initialization or by pulse order reversal, and are still competitive compared with HR and MHR schemes to a systematic imperfection in laser phase stepping process during the error signal reconstruction. We have indeed not considered other important technical problems such as local oscillator phase noise, rapid laser power fluctuation, or electronic servo bandwidth restriction which are out of the scope of this paper. However such noise sources should reduce the locked frequency stability but not necessarily its accuracy.

Our frequency measurement protocol might be applied to weakly allowed or forbidden atomic transitions and might be very useful for the next generation of 1D and 3D optical lattice clocks [50,51] probed by direct laser excitation or by high-power magic-wave-induced transitions [52], magnetically induced spectroscopy [21–23], or based on hyper-Raman Ramsey spectroscopy [53]. Laser spectroscopy protected against probe-field-induced frequency shifts will perform better high-resolution frequency measurements by suppressing spurious phase shifts from the excitation pulses in precision spectroscopy [54,55], Doppler-free two-photon spectroscopy [56–58], tracking the tiniest changes in molecular vibrational frequencies based on clocks sensitive to potential variation in the electron-to-proton mass ratio [59–62], fundamental physics tests and metrology with hydrogen molecular ions [63], future nuclear clocks based on γ transitions [64,65], observing some unexpected clock frequency shifts related to mass defect effects [66], and in the recent application of Ramsey-type mass spectrometry [67,68].

Thus, a new generation of optical generalized hyper-Ramsey quantum clocks may achieve an unprecedented breakthrough in extreme precision measurements for the next targeted 10^{-19} level of relative accuracy.

ACKNOWLEDGMENTS

T.Z.-W. deeply acknowledges E. de Clercq, E. Arimondo, C. J. Bordé, B. Darquié, M. Glass-Maujean, C. Janssen, M. H. Levitt, A. Ludlow, Y. Té, and J. Ye for suggestions and careful reading of the manuscript. V.I.Y. was supported by the Ministry of Education and Science of the Russian Federation (Project No. 3.1326.2017). A.V.T. was supported by the Russian Scientific Foundation (Project No. 16-12-00052).

APPENDIX A: TIME-DEPENDENT MATRIX ELEMENTS

The analytic solution of generalized composite laser pulses used to design our universal protocol is explicitly expressed along with an in-depth analysis of the error signal construction and how the proposed protocol exploits symmetrization to provide robustness against probe-induced frequency shifts and various dissipative processes. Some important results based on a combination of specific phase-modulated (GHR) resonances realize a very robust clock laser stabilization scheme against decoherence. The generalized hyper-Ramsey resonance is described within the density matrix formalism including decoherence. The optical Bloch equations presented in the main text [see Eq. (1)] describe the laser field interaction with a two-state quantum system. The general solution $M(\theta_l)$ is derived in a matrix form including $M_l(\infty)$ steady-state solutions written as [42,44]

$$\begin{aligned} M(\theta_l) &= R(\theta_l)[M_l(0) - M_l(\infty)] + M_l(\infty), \\ M_l(\infty) &= -\frac{\Gamma}{\mathcal{D}}\begin{pmatrix} \delta_l\Omega_l\cos\varphi_l - \gamma_c\Omega_l\sin\varphi_l \\ \gamma_c\Omega_l\cos\varphi_l + \delta_l\Omega_l\sin\varphi_l \\ \gamma_c^2 + \delta_l^2 \end{pmatrix}, \\ \mathcal{D} &= \gamma_c\Omega_l^2 + (\Gamma + 2\xi)\left(\gamma_c^2 + \delta_l^2\right), \end{aligned} \tag{A1}$$

where the clock frequency detuning is defined by $\delta_l = \delta - \Delta_l$ (Δ_l is the uncompensated part of the probe-induced frequency shift) and the generalized pulse area is $\theta_l = \omega_l\tau_l$. The square evolution matrix $R(\theta_l)$ requires exponentiation of the β_l matrix [Eq. (3)]. These square matrix elements $R_{mn}(\theta_l)$ following Refs. [44,46] are given by

$$\begin{aligned} R_{11}(\theta_l) &= e^{-\gamma_c\tau_l}\left(a_0 - a_2\left[\delta_l^2 + \Omega_l^2\sin^2\varphi_l\right]\right), \\ R_{12}(\theta_l) &= e^{-\gamma_c\tau_l}\left(a_1\delta_l + a_2\Omega_l^2\sin\varphi_l\cos\varphi_l\right), \\ R_{13}(\theta_l) &= e^{-\gamma_c\tau_l}(a_2[\delta_l\Omega_l\cos\varphi_l - \Delta\gamma\,\Omega_l\sin\varphi_l] \\ &\quad - a_1\Omega_l\sin\varphi_l), \\ R_{21}(\theta_l) &= e^{-\gamma_c\tau_l}\left(-a_1\delta_l + a_2\Omega_l^2\sin\varphi_l\cos\varphi_l\right), \\ R_{22}(\theta_l) &= e^{-\gamma_c\tau_l}\left(a_0 - a_2[\delta_l^2 + \Omega_l^2\cos^2\varphi_l]\right), \\ R_{23}(\theta_l) &= e^{-\gamma_c\tau_l}(a_2[\delta_l\Omega_l\sin\varphi_l + \Delta\gamma\,\Omega_l\cos\varphi_l] \\ &\quad + a_1\Omega_l\cos\varphi_l), \\ R_{31}(\theta_l) &= e^{-\gamma_c\tau_l}(a_2[\delta_l\Omega_l\cos\varphi_l + \Delta\gamma\,\Omega_l\sin\varphi_l] \\ &\quad + a_1\Omega_l\sin\varphi_l), \\ R_{32}(\theta_l) &= e^{-\gamma_c\tau_l}(a_2[\delta_l\Omega_l\sin\varphi_l - \Delta\gamma\,\Omega_l\cos\varphi_l] \\ &\quad - a_1\Omega_l\cos\varphi_l), \\ R_{33}(\theta_l) &= e^{-\gamma_c\tau_l}\left(a_0 + a_1\Delta\gamma - a_2\left[\Omega_l^2 - \Delta\gamma^2\right]\right), \end{aligned} \tag{A2}$$

where $\Delta\gamma = \gamma_c - (\Gamma + 2\xi)$. Auxiliary time-dependent functions $a_0 \equiv a_0(\theta_l), a_1 \equiv a_1(\theta_l), a_2 \equiv a_2(\theta_l)$ are given by [41,44]

$$\begin{aligned} a_0(\theta_l) &= [(SD_3 - TD_2)\sin\theta_l + (SD_2 + TD_3)\cos\theta_l]e^{\rho_l\tau_l} \\ &\quad + \left(D_0\eta_l + g_l^2\right)Re^{\eta_l\tau_l}, \\ a_1(\theta_l) &= [(SD_1 - T\omega_l)\sin\theta_l + (S\omega_l + TD_1)\cos\theta_l]e^{\rho_l\tau_l} \\ &\quad + D_0Re^{\eta_l\tau_l}, \\ a_2(\theta_l) &= [S\sin\theta_l + T\cos\theta_l]e^{\rho_l\tau_l} + Re^{\eta_l\tau_l}, \end{aligned} \tag{A3}$$

and relations between derivatives as [44]

$$\begin{aligned} \dot{a}_0(\theta_l) &= \delta_l^2\Delta\gamma\,a_2(\theta_l), \\ \dot{a}_1(\theta_l) &= a_0(\theta_l) - g_l^2a_2(\theta_l), \\ \dot{a}_2(\theta_l) &= a_1(\theta_l) + \Delta\gamma\,a_2(\theta_l), \end{aligned} \tag{A4}$$

with an auxiliary variable for convenience:

$$a_3(\theta_l) = a_0(\theta_l) - a_2(\theta_l)\delta_l^2. \tag{A5}$$

We introduce the following notation:

$$\begin{aligned} g_l^2 &= \Omega_l^2 + \delta_l^2, \\ D_0 &= \eta_l - \Delta\gamma, \\ D_1 &= \rho_l - \Delta\gamma, \\ D_2 &= \omega_l(2\rho_l - \Delta\gamma), \\ D_3 &= \left(\rho_l^2 - \omega_l^2 - \rho_l\Delta\gamma + g_l^2\right), \end{aligned} \tag{A6}$$

and

$$\begin{aligned} R &= \frac{1}{(\rho_l - \eta_l)^2 + \omega_l^2}, \\ S &= \frac{(\rho_l - \eta_l)}{\omega_l\left((\rho_l - \eta_l)^2 + \omega_l^2\right)}, \\ T &= \frac{-1}{(\rho_l - \eta_l)^2 + \omega_l^2}. \end{aligned} \tag{A7}$$

The three roots of the matrix (one real root η_l and two complex ones $\rho_l \pm i\omega_l$) are by Cardan's cubic solutions leading to damping terms η_l, ρ_l and a generalized angular frequency ω_l written as

$$\begin{aligned} \eta_l &= \frac{1}{3}\left(\Delta\gamma - C - \frac{\Delta_0}{C}\right), \\ \rho_l &= \frac{1}{3}\left(\Delta\gamma + \frac{C}{2} + \frac{\Delta_0}{2C}\right), \\ \omega_l &= \frac{\sqrt{3}}{6}\left(-C + \frac{\Delta_0}{C}\right), \\ \Delta_0 &= \Delta\gamma^2 - 3g_l^2, \\ \Delta_1 &= -2\Delta\gamma^3 + 9g_l^2\Delta\gamma - 27\delta_l^2\Delta\gamma, \\ C &= \sqrt[3]{\frac{\Delta_1 + \sqrt{\Delta_1^2 - 4\Delta_0^3}}{2}}. \end{aligned} \tag{A8}$$

APPENDIX B: CLOCK FREQUENCY SHIFT $\delta\nu$ FROM RESONANCE LINE SHAPES

Using exact analytic expressions to solve the Bloch equations for a single given Rabi pulse, the expression for a full sequence of n pulses can be generalized to

$$M(\theta_1, \ldots, \theta_n) = \sum_{p=1}^{n}\left[\left(\prod_{l=p}^{\overleftarrow{n}} R(\theta_l)\right)[M_{p-1}(\infty) - M_p(\infty)]\right] + M_n(\infty), \tag{B1}$$

where state initialization means $M_0(\infty) \equiv M_1(0)$ by convention. Such an expression can be rewritten to the canonical form presented in the paper [see Eq. (5)] using some phasor expressions while fixing index k for the free evolution time. Any composite laser-pulse sequence can indeed be recast such as

$$M(\theta_1, \ldots, \theta_n) \equiv A + B(\Phi)\cos(\delta T + \Phi), \tag{B2}$$

as long as we consider a unique pulse switching off the laser field used as a pivot in the factorization process. The population transfer $P_{|g\rangle\mapsto|e\rangle}$ is related to the third component of the Bloch components $M(\theta_1, \ldots, \theta_n)$ as

$$P_{|g\rangle\mapsto|e\rangle} = \frac{1 + W(\theta_1, \ldots, \theta_n)}{2}. \tag{B3}$$

To establish the frequency shift of the resonance curve associated with the population transfer $P_{|g\rangle\mapsto|e\rangle}$, tracking the extremum of Eq. (B2) is required. The condition is given by $\partial P_{|g\rangle\mapsto|e\rangle}/\partial\delta|_{\delta\to 0} = 0$ which leads to the first-order expression as

$$\delta\nu = -\frac{\Phi|_{\delta\to 0}}{2\pi(T + \partial_\delta\Phi|_{\delta\to 0})}, \tag{B4}$$

where ∂_δ means a derivation with respect to the unperturbed clock detuning δ. When high-order corrections are taken into account in Eq. (B4), the phase shift has to be replaced by $\Phi \mapsto \Phi + \Psi + \Theta$ where

$$\Psi = -\arctan\left[\frac{\partial_\delta B(\Phi)}{(T + \partial_\delta\Phi)B(\Phi)}\right], \tag{B5a}$$

$$\Theta = \arcsin\left[\frac{\partial_\delta A}{\sqrt{[\partial_\delta B(\Phi)]^2 + [(T + \partial_\delta\Phi)B(\Phi)]^2}}\right]. \tag{B5b}$$

High-order terms given by Eq. (B5a) and Eq. (B5b) can handle a possible distortion of the line shape when the free evolution time T is not so large compared to pulse duration.

APPENDIX C: CLOCK FREQUENCY SHIFT $\delta\widetilde{\nu}$ FROM ERROR SIGNAL LINE SHAPES

The error signal given by Eq. (11) used to lock the laser frequency is generated by taking the difference between two phase-modulated resonances as

$$\Delta E = P_{|g\rangle\mapsto|e\rangle}(\varphi_{l+}) - P_{|g\rangle\mapsto|e\rangle}(\varphi_{l-}). \tag{C1}$$

For instance the shift $\delta\nu$ of the frequency locking point from the error signal due to an imperfect light-shift compensation is given by the relation

$$\Delta E|_{\delta=\delta\widetilde{\nu}} = 0. \tag{C2}$$

To evaluate the clock frequency shift associated with different phase-step modulations, we use Eq. (C2) to determine the analytical form of the frequency-shifted locking point as

$$\delta\widetilde{\nu} = \frac{1}{2\pi T}\left(-\widetilde{\Phi}|_{\delta\to 0} \pm \arccos\left[-\frac{\widetilde{A}|_{\delta\to 0}}{\widetilde{B}(\widetilde{\Phi})|_{\delta\to 0}}\right]\right) \tag{C3}$$

with a new phase-shift expression:

$$\widetilde{\Phi} = \arctan\left[\frac{B(\Phi)_{(\varphi_{l+})}\sin\Phi_{(\varphi_{l+})} - B(\Phi)_{(\varphi_{l-})}\sin\Phi_{(\varphi_{l-})}}{B(\Phi)_{(\varphi_{l+})}\cos\Phi_{(\varphi_{l+})} - B(\Phi)_{(\varphi_{l-})}\cos\Phi_{(\varphi_{l-})}}\right] \tag{C4}$$

including new offset and amplitude parameters as

$$\begin{aligned} \widetilde{A} &= A_{(\varphi_{l+})} - A_{(\varphi_{l-})}, \\ \widetilde{B}(\widetilde{\Phi}) &= [B(\Phi)_{(\varphi_{l+})}\cos\Phi_{(\varphi_{l+})} - B(\Phi)_{(\varphi_{l-})}\cos\Phi_{(\varphi_{l-})}] \\ &\quad \times\sqrt{1 + \tan^2\widetilde{\Phi}}. \end{aligned} \tag{C5}$$

APPENDIX D: ERROR SIGNAL $\Delta E_{\Downarrow\Uparrow}$ ($\Delta E^{\dagger}_{\Downarrow\Uparrow}$) LINE SHAPE

The proposed universal protocol interleaving $\pm\pi/4$ and $\pm 3\pi/4$ laser-phase steps with a Bloch-vector initialization in each quantum state allows for an exact cancellation of all cosine terms in the error signal pattern. It is leaving a pure dispersive signal $\Delta E \equiv \Delta E[\mathrm{GHR}(\pi/4,3\pi/4)]$ while providing a perfectly robust locking point at the unperturbed clock frequency $\delta = 0$ against residual probe-induced frequency shifts. The error signal shape is evaluated explicitly based on a GHR protocol defined by 4 composite pulses (θ_l) ($l = 1,2,3,4$) where phase steps are applied only within θ_3 and with a free evolution time when $l = k = 2$ fixing $\theta_2 = \delta T$. Due to pulse parameters that are defined by $\delta_l \equiv \delta - \Delta$ during laser interaction, $\Omega_l \equiv \Omega = \pi/2\tau$, and a choice of successive pulse durations as $\tau, T, 2\tau, \tau$, a standard relation $R(\theta_1) = R(\theta_4)$ is obtained.

The dispersive error signal ΔE based on Fig. 4(a) is then computed by successive differences between Bloch-vector components alternating negative and positive $\varphi_3 = \pi/4, 3\pi/4$ phase steps reducing to the compact expression

$$\Delta E = R(\theta_1)\Delta R(\theta_3)R(\delta T)M(\theta_1), \tag{D1}$$

where we have introduced

$$\Delta R(\theta_3) = R(\theta_3)_{(+\frac{\pi}{4})} - R(\theta_3)_{(-\frac{\pi}{4})} - \left[R(\theta_3)_{(+3\frac{\pi}{4})} - R(\theta_3)_{(-3\frac{\pi}{4})}\right]. \tag{D2}$$

Bloch-vector component initialization for the first pulse is here $M_1(0) = (0,0,W(0))$. Note that successive differences between $M_{l_{(\pm\varphi_l)}}$ steady states and from cross-product terms of the form $R(\theta_3)_{(\pm\varphi_l)}M_{l_{(\pm\varphi_l)}}$ cancel together exactly due to the particular choice of phase steps.

When steady states are vanishing $M_l(\infty) \equiv 0$, Eq. (D1) can be directly reduced to the single product expression:

$$\Delta E = R(\theta_1)\Delta R(\theta_3)R(\delta T)R(\theta_1)M_1(0). \tag{D3}$$

A symmetrization occurs for $\Delta R(\theta_3)$ and comes from exploiting $\pm\pi/4, \pm 3\pi/4$ phase combinations between successive sequences of composite laser pulses, $\varphi \to -\varphi$ for cosine terms and $\varphi \to \pi - \varphi$ for sine terms, leading to a simple Pauli-like matrix:

$$\Delta R(\theta_3) = 2a_2(\theta_3)e^{-2\gamma_c\tau}\Omega^2 \begin{pmatrix} 0 & 1 & 0 \\ 1 & 0 & 0 \\ 0 & 0 & 0 \end{pmatrix}. \tag{D4}$$

The final compact expression of the error signal is rewritten as

$$\Delta E = AW(0)\begin{pmatrix} C_u\cos(\delta T) + S_u\sin(\delta T) \\ C_v\cos(\delta T) + S_v\sin(\delta T) \\ -S_w\sin(\delta T) \end{pmatrix}, \tag{D5}$$

where $A = 2a_2(\theta_3)\Omega^2 e^{-\gamma_c(4\tau+T)}$. Matrix elements $S_{u,v,w}$ and $C_{u,v,w}$ are reduced in a compact form using relations from Eq. (A4) as

$$\begin{aligned} S_u &= \Omega\delta_1[a_1(\theta_1)\dot{a}_2(\theta_1) - a_3(\theta_1)a_2(\theta_1)], \\ S_v &= \Omega\left[\dot{a}_1(\theta_1)\dot{a}_2(\theta_1) + a_1(\theta_1)a_2(\theta_1)\delta_1^2\right], \\ S_w &= \Omega^2\left[[\dot{a}_2(\theta_1)]^2 + a_2(\theta_1)^2\delta_1^2\right], \\ C_u &= \Omega\left[a_1(\theta_1)a_2(\theta_1)\delta_1^2 + a_3(\theta_1)\dot{a}_2(\theta_1)\right], \\ C_v &= \Omega\delta_1[\dot{a}_1(\theta_1)a_2(\theta_1) - a_1(\theta_1)\dot{a}_2(\theta_1)], \\ C_w &= 0, \end{aligned} \tag{D6}$$

with the unperturbed clock detuning corrected by probe-induced shifts as $\delta_1 = \delta - \Delta$.

The normalized error signal connected to the third Bloch-vector component $\Delta E_{\Downarrow(\Uparrow)} \equiv \Delta E(W)_{\Downarrow(\Uparrow)}$ is extracted by taking differences between several population excitation fraction measurements. When only a decoherence term γ_c is active, all steady states are indeed vanishing. The normalized error signal is given by Eq. (13) with population initialization in either ground state $|g\rangle \equiv \Downarrow$ or excited state $|e\rangle \equiv \Uparrow$. We then have

$$\Delta E_{\Downarrow(\Uparrow)} = -\tfrac{1}{4}A_{\Downarrow(\Uparrow)}(0)\left[\dot{a}_2(\theta_1)^2 + a_2(\theta_1)^2\delta_1^2\right]\sin(\delta T), \tag{D7}$$

with $A_{\Downarrow(\Uparrow)}(0) = \Omega^2 AW(0)$ and where we apply $W(0)_{\Downarrow(\Uparrow)} = -1\ (+1)$ respectively. This is always a dispersive curve centered at the unperturbed optical clock frequency which is completely free from probe-induced frequency shifts at all orders.

When the decoherence term γ_c and relaxation terms Γ, ξ are simultaneously present, steady states are nonvanishing. However, when two sets of Eq. (D1) interleaved by population initialization in both states are applied, the difference following Eq. (14) gives an identical error signal expression eliminating steady states as

$$\Delta E_{\Downarrow\Uparrow} = -\tfrac{1}{8}A_{\Downarrow\Uparrow}(0)\left[\dot{a}_2(\theta_1)^2 + a_2(\theta_1)^2\delta_1^2\right]\sin(\delta T), \tag{D8}$$

with $A_{\Downarrow(\Uparrow)}(0) = \Omega^2 A(W(0)_{\Downarrow} - W(0)_{\Uparrow})$. The resulting dispersive pattern versus the unperturbed clock frequency detuning δ is given by Eq. (D8) taking $W(0)_{\Downarrow(\Uparrow)} = -1\ (+1)$ for a full population inversion between quantum states.

It is also possible to read the sequence of composite pulses from left to right or from right to left by applying a time-reversal symmetry $t \to -t$ and phase inversion $\varphi \to -\varphi$ on the diagram shown in Fig. 4(a) leading to another equivalent scheme presented in Fig. 4(b). We derive an alternative error signal called $\Delta E^{\dagger}$, following the mirror-like protocol shown in Fig. 4(b). We simply apply a permutation of laser parameters between pulse areas $\theta_2 \leftrightarrow \theta_3$ still keeping $R(\theta_1) = R(\theta_4)$ which directly leads to another error signal expression as

$$\Delta E^{\dagger} = -R(\theta_1)R(\delta T)\Delta R(\theta_3)M(\theta_1). \tag{D9}$$

We still generate the normalized error signal $\Delta E^{\dagger}_{\Downarrow(\Uparrow)}$ following Eq. (13) when only decoherence is present or the normalized error signal $\Delta E^{\dagger}_{\Downarrow\Uparrow}$ following Eq. (14) when decoherence and relaxation are both activated. We obtain error signal line shapes that are identical to Eqs. (D5)–(D8).

APPENDIX E: ERROR SIGNAL $\Delta\overline{E}_{\Downarrow\Downarrow}$ LINE SHAPE

An ultimate ultrastable universal interrogation protocol interleaving $\pm\pi/4$ and $\pm 3\pi/4$ laser phase steps with a Bloch-vector initialization in only one single quantum state allows for an exact cancellation of all cosine terms in the error signal pattern. We show here that by combining two GHR protocols with a sequence of composite pulses that are reversed in time ordering, as shown in Fig. 4(c), similar dispersive shapes are recovered eliminating population initialization in the upper state. We focus on the ultrastable error signal which relies on a combination of ΔE and $\Delta E^{\dagger}$ based on the protocol reported in Fig. 4(c). We obtain a dispersive line shape that does not require initialization population in both states, even insensitive to nonvanishing real and imaginary part of any initial optical coherence $U(0), V(0) \neq 0$ when starting the interrogation protocol, as follows:

$$\Delta\overline{E} \equiv \Delta E + \Delta E^{\dagger} = R(\theta_1)\Delta R(\theta_3,\delta T)M(\theta_1), \tag{E1}$$

where the commutator is $\Delta R(\theta_3,\delta T) = [\Delta R(\theta_3), R(\delta T)]$. We derive exact expressions for matrix components as

$$\Delta\overline{E} = A\begin{pmatrix} -\left[a_1(\theta_1)^2\delta_1^2 + a_3(\theta_1)^2\right]U(0) - S_1V(0) + S_2W(0) - \frac{\Gamma\Omega\delta_1}{\mathcal{D}}[-a_3(\theta_1)S_4 + a_1(\theta_1)S_5] \\ S_1U(0) + \left[a_1(\theta_1)^2\delta_1^2 + \dot{a}_1(\theta_1)^2\right]V(0) + S_3W(0) - \frac{\Gamma\Omega}{\mathcal{D}}\left[a_1(\theta_1)\delta_1^2S_4 + \dot{a}_1(\theta_1)S_5\right] \\ S_2U(0) - S_3V(0) - \Omega^2\left[\dot{a}_2(\theta_1)^2 + a_2(\theta_1)^2\delta_1^2\right]W(0) + \frac{\Gamma\Omega^2}{\mathcal{D}}\left[a_2(\theta_1)\delta_1^2S_4 + \dot{a}_2(\theta_1)S_5\right] \end{pmatrix}\sin(\delta T), \tag{E2}$$

with $A = 4a_2(\theta_3)\Omega^2e^{-\gamma_c(4\tau+T)}$. We demonstrate that protocol shown in Fig. 4(c) is even more robust than protocols shown Figs. 4(a) and 4(b) because all Bloch-vector matrix components are multiplied by a sine term eliminating uncompensated probe-induced frequency shifts.

We introduce reduced variables S_i $(i = 1,2,3,4,5)$ as follows:

$$\begin{aligned} &S_1 = a_1(\theta_1)\delta_1[a_3(\theta_1) - \dot{a}_1(\theta_1)], \quad S_2 = \Omega\delta_1[a_1(\theta_1)\dot{a}_2(\theta_1) - a_2(\theta_1)a_3(\theta_1)], \quad S_3 = \Omega[a_1(\theta_1)a_2(\theta_1)\delta_1^2 + \dot{a}_1(\theta_1)\dot{a}_2(\theta_1)], \\ &S_4 = e^{\gamma_c\tau} - a_3(\theta_1) - a_1(\theta_1)\gamma_c - a_2(\theta_1)\left(\gamma_c^2 + \delta_1^2\right), \quad S_5 = a_1(\theta_1)\delta_1^2 + \gamma_c[e^{\gamma_c\tau} - \dot{a}_1(\theta_1)] - \dot{a}_2(\theta_1)\left(\gamma_c^2 + \delta_1^2\right). \end{aligned} \tag{E3}$$

We finally derive a new ultrastable normalized error signal $\Delta\overline{E}_{\Downarrow\Downarrow}$ based on population transfer following Eq. (15) with $U(0) = V(0) = 0$ as

$$\Delta\overline{E}_{\Downarrow\Downarrow} = -\frac{1}{8}A\Omega^2\left[\left[\dot{a}_2(\theta_1)^2 + a_2(\theta_1)^2\delta_1^2\right]W(0)_{\Downarrow\Downarrow} - \frac{\Gamma}{\mathcal{D}}\left[a_2(\theta_1)\delta_1^2S_4 + \dot{a}_2(\theta_1)S_5\right]\right]\sin(\delta T). \tag{E4}$$

The resulting dispersive pattern versus the unperturbed clock frequency detuning δ is given by Eq. (E4) taking only $W(0)_{\Downarrow\Downarrow} = -1$. If we neglect a small correction on signal contrast due to decoherence and relaxation terms in Eq. (E4), we retrieve a line-shape expression which is identical to Eq. (D7) and Eq. (D8) and does not require a population inversion between quantum states.

[1] A. D. Ludlow, M. M. Boyd, J. Ye, E. Peik, and P. O. Schmidt, Optical atomic clocks, Rev. Mod. Phys. **87**, 637 (2015).

[2] C. W. Chou, D. B. Hume, T. Rosenband, and D. J. Wineland, Optical clocks and relativity, Science **329**, 1630 (2010).

[3] V. A. Dzuba and V. V. Flambaum, Limits on gravitational Einstein equivalence principle violation from monitoring atomic clock frequencies during a year, Phys. Rev. D **95**, 015019 (2017).

[4] S. Kolkowitz, I. Pikowski, N. Langellier, M. D. Lukin, R. L. Walsworth, and J. Ye, Gravitational wave detection with optical lattice atomic clocks, Phys. Rev. D **94**, 124043 (2016).

[5] J.-P. Uzan, The stability of fundamental constants, C. R. Phys. **16**, 576 (2015).

[6] A. Derenvienko, Atomic clocks and dark-matter signatures, J. Phys.: Conf. Ser. **723**, 012043 (2016).

[7] C. W. Chou, D. B. Hume, J. C. J. Koelemeij, D. J. Wineland, and T. Rosenband, Frequency Comparison of Two High-Accuracy Al^+ Optical Clocks, Phys. Rev. Lett. **104**, 070802 (2010).

[8] H. S. Margolis, Trapped ion optical clocks, Eur. Phys. J.: Spec. Top. **172**, 97 (2009).

[9] J. Ye, H. J. Kimble, and H. Katori, Quantum state engineering and precision metrology using state-insensitive light traps, Science **320**, 1734 (2008).

[10] A. Derevianko and H. Katori, Colloquium: Physics of optical lattice clocks, Rev. Mod. Phys. **83**, 331 (2011).

[11] H. Katori, Optical lattice clocks and quantum metrology, Nat. Photon. **5**, 203 (2011).

[12] P. O. Schmidt, T. Rosenband, C. Langer, W. M. Itano, J. C. Bergquist, and D. J. Wineland, Spectroscopy using quantum logic, Science **309**, 749 (2005).

[13] N. Huntemann, C. Sanner, B. Lipphardt, Chr. Tamm, and E. Peik, Single-Ion Atomic Clock with 3×10^{-18} Systematic Uncertainty, Phys. Rev. Lett. **116**, 063001 (2016).

[14] M. Schioppo, R. C. Brown, W. F. McGrew, N. Hinkley, R. J. Fasano, K. Beloy, T. H. Yoon, G. Milani, D. Nicolodi, J. A. Sherman, N. B. Phillips, C. W. Oates, and A. D. Ludlow, Ultrastable optical clock with two cold-atom ensembles, Nat. Photon. **11**, 48 (2017).

[15] T. L. Nicholson, S. L. Campbell, R. B. Hutson, G. E. Marti, B. J. Bloom, R. L. McNally, W. Zhang, M. D. Barrett, M. S. Safronova, G. F. Strouse, W. L. Tew, and J. Ye, Systematic evaluation of an atomic clock at 2×10^{-18} total uncertainty, Nat. Commun. **6**, 7896 (2015).

[16] R. Le Targat, L. Lorini, Y. Le Coq, M. Zawada, J. Guéna, M. Abgrall, M. Gurov, P. Rosenbusch, D. G. Rovera, B. Nagórny, R. Gartman, P. G. Westergaard, M. E. Tobar, M. Lours,

G. Santarelli, A. Clairon, S. Bize, P. Laurent, P. Lemonde, and J. Lodewyck, Experimental realization of an optical second with strontium lattice clocks, Nat. Commun. **4**, 2109 (2013).

[17] F. Riehle, Towards a redefinition of the second based on optical atomic clocks, C. R. Phys. **16**, 506 (2015).

[18] R. Santra, E. Arimondo, T. Ido, C. H. Greene, and J. Ye, High-Accuracy Optical Clock via Three-Level Coherence in Neutral Bosonic ^{88}Sr, Phys. Rev. Lett. **94**, 173002 (2005).

[19] T. Zanon-Willette, A. D. Ludlow, S. Blatt, M. M. Boyd, E. Arimondo, and J. Ye, Cancellation of Stark Shifts in Optical Lattice Clocks by Use of Pulsed Raman and Electromagnetically Induced Transparency Techniques, Phys. Rev. Lett. **97**, 233001 (2006).

[20] A. V. Taichenachev, V. I. Yudin, C. W. Oates, C. W. Hoyt, Z. W. Barber, and L. Hollberg, Magnetic Field-Induced Spectroscopy of Forbidden Optical Transitions with Application to Lattice-Based Optical Atomic Clocks, Phys. Rev. Lett. **96**, 083001 (2006).

[21] Z. Barber, C. Hoyt, C. Oates, L. Hollberg, A. Taichenachev, and V. Yudin, Direct Excitation of the Forbidden Clock Transition in Neutral ^{174}Yb Atoms Confined to an Optical Lattice, Phys. Rev. Lett. **96**, 083002 (2006).

[22] X. Baillard, M. Fouché, R. Le Targat, P. G. Westergaard, A. Lecallier, Y. Le Coq, G. D. Rovera, S. Bize, and P. Lemonde, Accuracy evaluation of an optical lattice clock with bosonic atoms, Opt. Lett. **32**, 1812 (2007).

[23] A. P. Kulosa, D. Fim, K. H. Zipfel, S. Rühmann, S. Sauer, N. Jha, K. Gibble, W. Ertmer, E. M. Rasel, M. S. Safronova, U. I. Safronova, and S. G. Porsev, Towards a Mg Lattice Clock: Observation of the $^1S_0$-$^3P_0$ Transition and Determination of the Magic Wavelength, Phys. Rev. Lett. **115**, 240801 (2015).

[24] N. F. Ramsey, *Molecular Beams* (Clarendon Press, Oxford, 1956).

[25] A. V. Taichenachev, V. I. Yudin, C. W. Oates, Z. W. Barber, N. D. Lemke, A. D. Ludlow, U. Sterr, Ch. Lisdat, and F. Riehle, Compensation of field-induced frequency shifts in Ramsey spectroscopy of optical clock transitions, JETP. Lett. **90**, 713 (2009).

[26] M. H. Levitt, Composite pulses, Prog. Nucl. Magn. Reson. Spectrosc. **18**, 61 (1986).

[27] L. M. K. Vandersypen and I. L. Chuang, NMR techniques for quantum control and computation, Rev. Mod. Phys. **76**, 1037 (2005).

[28] M. Braun and S. J. Glaser, Concurrently optimized cooperative pulses in robust quantum control: Application to broadband Ramsey-type pulse sequence elements, New J. Phys. **16**, 115002 (2014).

[29] N. F. Ramsey and H. B. Silsbee, Phase shifts in the molecular beam method of separated oscillating fields, Phys. Rev. **84**, 506 (1951).

[30] A. Morinaga, F. Riehle, J. Ishikawa, and J. Helmcke, A Ca optical frequency standard: Frequency stabilization by means of nonlinear Ramsey resonances, Appl. Phys. B **48**, 165 (1989); IEEE Trans. Instrum. Meas. **38**, 524 (1989).

[31] V. Letchumanan, P. Gill, A. G. Sinclair, and E. Riis, Optical-clock local-oscillator stabilization scheme, J. Opt. Soc. Am. B **23**, 714 (2006).

[32] V. I. Yudin, A. V. Taichenachev, C. W. Oates, Z. W Barber, N. D. Lemke, A. D. Ludlow, U. Sterr, Ch. Lisdat, and F. Riehle, Hyper-Ramsey spectroscopy of optical clock transitions, Phys. Rev. A **82**, 011804(R) (2010).

[33] T. Zanon-Willette, V. I. Yudin, and A. V. Taichenachev, Generalized hyper-Ramsey resonance with separated oscillating fields, Phys. Rev. A **92**, 023416 (2015).

[34] T. Zanon-Willette, E. de Clercq, and E. Arimondo, Probe light-shift elimination in generalized hyper-Ramsey quantum clocks, Phys. Rev. A **93**, 042506 (2016).

[35] T. Zanon-Willette, M. Minissale, V. I. Yudin, and A. V. Taichenachev, Composite pulses in hyper-Ramsey spectroscopy for the next generation of atomic clocks, J. Phys.: Conf. Ser. **723**, 012057 (2016).

[36] N. Huntemann, B. Lipphardt, M. Okhapkin, Chr. Tamm, E. Peik, A. V. Taichenachev, and V. I. Yudin, Generalized Ramsey Excitation Scheme with Suppressed Light Shift, Phys. Rev. Lett. **109**, 213002 (2012).

[37] R. Hobson, W. Bowden, S. A. King, P. E. G. Baird, I. R. Hill, and P. Gill, Modified hyper-Ramsey methods for the elimination of probe shifts in optical clocks, Phys. Rev. A **93**, 010501(R) (2016).

[38] V. I. Yudin, A. V. Taichenachev, M. Yu. Basalaev, and T. Zanon-Willette, Synthetic frequency protocol for Ramsey spectroscopy of clock transitions, Phys. Rev. A **94**, 052505 (2016).

[39] K. S. Tabatchikova, A. V. Taichenachev, and V. I. Yudin, Generalized Ramsey scheme for precision spectroscopy of ultracold atoms and ions: Inclusion of a finite laser line width and spontaneous relaxation of the atomic levels, JETP Lett. **97**, 311 (2013).

[40] K. S. Tabatchikova, A. V. Taichenachev, A. K. Dmitriev, and V. I. Yudin, Study of field shifts of Ramsey resonances on ultracold atoms and ions, JETP Lett. **120**, 203 (2015).

[41] H. C. Torrey, Transient nutations in nuclear magnetic resonance, Phys. Rev. **76**, 1059 (1949).

[42] E. T. Jaynes, Matrix treatment of nuclear induction, Phys. Rev. **98**, 1099 (1955).

[43] L. Allen and J. H. Eberly, *Optical Resonance and Two-Level Atoms* (John Wiley and Sons, Inc., New York, 1975).

[44] R. L. Schoemaker, in *Laser Coherence Spectroscopy*, edited by J. I. Steinfeld (Plenum Press, New York, 1978).

[45] C. Cohen-Tannoudji, J. Dupont-Roc, and G. Grynberg, *Atom-Photon Interactions: Basic Processes and Applications* (Wiley, New York, 1992).

[46] P. R. Berman and V. S. Malinovsky, *Principles of Laser Spectroscopy and Quantum Optics* (Princeton University Press, Princeton, NJ, 2011).

[47] T. R. Tan, J. P. Gaebler, Y. Lin, Y. Wan, R. Bowler, D. Leibfried, and D. J. Wineland, Multi-element logic gates for trapped-ion qubits, Nature (London) **528**, 380 (2015).

[48] E. L. Hahn, Spin echoes, Phys. Rev. **80**, 580 (1950).

[49] J. D. Prestage and S. K. Chung, Repetitive interrogation of 2-level quantum systems, in *Proceedings of the 2010 IEEE International Frequency Control Symposium* (IEEE, Newport Beach, CA, 2010), p. 220.

[50] T. Akatsuka, M. Takamoto, and H. Katori, Three-dimensional optical lattice clock with bosonic ^{88}Sr atoms, Phys. Rev. A **81**, 023402 (2010).

[51] S. L. Campbell, R. B. Hutson, G. E. Marti, A. Goban, N. Darkwah Oppong, R. L. McNally, L. Sonderhouse, J. M. Robinson, W. Zhang, B. J. Bloom, and J. Ye, A Fermi-degenerate three-dimensional optical lattice clock, arXiv:1702.01210.

[52] V. D. Ovsiannikov, V. G. Pal'chikov, A. V. Taichenachev, V. I. Yudin, H. Katori, and M. Takamoto, Magic-wave-induced $^1S_0$-$^3P_0$ transition in even isotopes of alkaline-earth-metal-like atoms, Phys. Rev. A **75**, 020501(R) (2007).

[53] T. Zanon-Willette, S. Almonacil, E. de Clercq, A. D. Ludlow, and E. Arimondo, Quantum engineering of atomic phase shifts in optical clocks, Phys. Rev. A **90**, 053427 (2014).

[54] O. Arnoult, F. Nez, L. Julien, and F. Biraben, Optical frequency measurement of the 1S-3S two-photon transition in hydrogen, Eur. Phys. J. D **60**, 243 (2010).

[55] A. Matveev, C. G. Parthey, K. Predehl, J. Alnis, A. Beyer, R. Holzwarth, T. Udem, T. Wilken, N. Kolachevsky, M. Abgrall, D. Rovera, C. Salomon, P. Laurent, G. Grosche, O. Terra, T. Legero, H. Schnatz, S. Weyers, B. Altschul, and T. W. Hänsch, Precision Measurement of the Hydrogen 1S-2S Frequency via a 920-km Fiber Link, Phys. Rev. Lett. **110**, 230801 (2013).

[56] C. Cohen-Tannoudji, Effect of a non-resonant irradiation on atomic energy levels: Application to light shifts in two-photon spectroscopy and to perturbation of Rydberg states, Metrologia **13**, 161 (1977).

[57] M. M. Salour and C. Cohen-Tannoudji, Observation of Ramsey's Interference Fringes in the Profile of Doppler-Free Two-Photon Resonances, Phys. Rev. Lett. **38**, 757 (1977).

[58] C. Bordé, Density matrix equations and diagrams for high-resolution nonlinear laser spectroscopy: Application to Ramsey fringes in the optical domain, in *Advances in Laser Spectroscopy*, edited by F. T. Arecchi, F. Strumia, and H. Walther (Plenum Press, New York, 1983).

[59] A. Derevianko, V. A. Dzuba, and V. V. Flambaum, Highly Charged Ions as a Basis of Optical Atomic Clockwork of Exceptional Accuracy, Phys. Rev. Lett. **109**, 180801 (2012).

[60] M. S. Safronova, V. A. Dzuba, V. V. Flambaum, U. I. Safronova, S. G. Porsev, and M. G. Kozlov, Highly Charged Ag-Like and In-Like Ions for the Development of Atomic Clocks and the Search for α Variation, Phys. Rev. Lett. **113**, 030801 (2014).

[61] S. Schiller, D. Bakalov, and V. I. Korobov, Simplest Molecules as Candidates for Precise Optical Clocks, Phys. Rev. Lett. **113**, 023004 (2014).

[62] V. I. Yudin, A. V. Taichenachev, and A. Derevianko, Magnetic-Dipole Transitions in Highly Charged Ions as a Basis of Ultraprecise Optical Clocks, Phys. Rev. Lett. **113**, 233003 (2014).

[63] J.-Ph. Karr, S. Patra, J. C. J. Koelemeij, J. Heinrich, N. Sillitoe, A. Douillet, and L. Hilico, Hydrogen molecular ions: New schemes for metrology and fundamental physics tests, J. Phys.: Conf. Ser. **723**, 012048 (2016).

[64] C. J. Campbell, A. G. Radnaev, A. Kuzmich, V. A. Dzuba, V. V. Flambaum, and A. Derevianko, Single-Ion Nuclear Clock for Metrology at the 19th Decimal Place, Phys. Rev. Lett. **108**, 120802 (2012).

[65] E. Peik and M. Okhapkin, Nuclear clocks based on resonant excitation of γ transitions, C. R. Phys. **16**, 516 (2015).

[66] V. I. Yudin and A. V. Taichenachev, Mass defect effects in atomic clocks, arXiv:1703.05290.

[67] M. Eibach, T. Beyer, K. Blaum, M. Block, K. Eberhardt, F. Herfurth, J. Ketelaer, Sz. Nagy, D. Neidherr, W. Nörtershäuser, and C. Smorra, First investigation of phase-shifted Ramsey excitation in Penning trap mass spectrometry, Int. J. Mass Spectrom. **303**, 27 (2011).

[68] S. George, K. Blaum, M. Block, M. Breitenfeldt, M. Dworschak, F. Herfurth, A. Herlert, M. Kowalska, M. Kretzschmar, E. Minaya Raminez, D. Neidherr, S. Scharwz, and L. Schweikhard, Damping effects in Penning trap mass spectrometry, Int. J. Mass Spectrom. **299**, 102 (2011).